Structural Biology and Molecular Biophysics

Free energy landscapes of KcsA inactivation

Sergio Pérez-Conesa, Lucie Delemotte

Science for Life Laboratory, Department of Applied Physics, KTH Royal Institute of Technology, Stockholm

Reviewed Preprint

Published from the original preprint after peer review and assessment by eLife.

About eLife's process

Reviewed preprint posted
July 4, 2023 (this version)

Sent for peer review
April 11, 2023

Posted to bioRxiv
April 6, 2023

Abstract

The bacterial ion channel KcsA has become a useful model of complex K+-ion channels thanks to its single pore domain structure whose sequence shares many similarities with eukaryotic channels. Like many physiologically-relevant ion channels, KcsA inactivates after prolonged exposure to stimuli (in this case, a lowered pH). The inactivation mechanism has been heavily investigated, using structural, functional and simulations methods, but the molecular basis underlying the energetics of the process remains actively debated. In this work, we use the “string method with swarms of trajectories” enhanced sampling technique to characterize the free energy landscape lining the KcsA inactivation process. After channel opening following a pH drop, KcsA presents metastable open states leading to an inactivated state. The final inactivation step consists of a constriction of the selectivty filter and entry of three water molecules into binding sites behind each selectivity filter subunit. Based our simulations, we propose a key role for residue L81 in opening a gateway for water molecules to enter their buried sites, rather than for Y82 which has previously been suggested to act as a lid. In addition, since we found the energetically favored inactivation mechanism to be dependent on the force field, our results also address the importance of parameter choice for this type of mechanism. In particular, inactivation involves passing through the fully-open state only when using the AMBER force field. In contrast, using CHARMM, selectivity filter constriction proceeds directly from the partially open state. Finally, our simulations suggest that removing the co-purifying lipids stabilizes the partially open states, rationalizing their importance for the proper inactivation of the channel.

eLife assessment

In this **valuable** study, advanced simulation methodologies are used to extract the mechanisms of inactivation for the potassium ion channel KcsA. The string method approach provides **solid** evidence that reveal features associated with the interplay between gate size and collapse of the selectivity filter, as well as remarkable differences between different force fields. While this manuscript does not address recent discoveries in K channel inactivation involving dilated selectivity filter structures obtained by Xray and cryo-EM, it does help us understand the KcsA constriction process. With added descriptions and analysis of collective variables, improved reproducibility of results, consistency between string method free energies and unbiased simulations, and improved transition rate calculation, this manuscript will be of interest to the ion channel field.

Introduction

The bacterial ion channel KcsA has become a standard model for complex eukaryotic K-ion channels due to the highly conserved nature of its sequence and the relative simplicity of its structure consisting of a single pore domain (***Figure 1a-b***). Indeed, the characteristic TVGYG sequence of the selectivity filter plays an important role in determining channel selectivity(***Doyle et al., 1998***). When the homotetramer is formed, the selectivity filter has four potassium binding sites (S1 to S4) which select for K+ over Na+ with a remarkable selectivity (***Figure 1a***). KcsA features two main regions where the flow of ions can be interrupted: the helical bundle crossing of TM2 or inner gate (IG) and the selectivity filter (SF), which can stop ion flow through its constriction at the level of residue G77(***Li et al., 2018***). One of the hallmarks of ion channel biochemistry is channel inactivation after prolonged exposure to the opening stimulus (***Hille, 2001***). This mechanism is essential to many physiological signaling mechanisms. In KcsA, the inactivation mechanism appears fairly established (***Li et al., 2018***), largely on the basis of numerous X-Ray diffraction structures (***Figure 1a-d***) (***Doyle et al., 1998***; ***Cuello et al., 2010a,b***, ***2017***). Upon exposure to low pH, the inner gate opens, allowing current to flow through the channel. The protein then visits millisecond-lived metastable states of increasing degrees of inner gate opening (***Figure 1b***), until an allosteric signal is transmitted from the inner gate to the selectivity filter causing it to constrict, ceasing the current and forming the inactivated state (***Figure 1c***). In this way, the selectivity filter acts as a secondary gate which is allosterically connected to the inner gate. In the conductive state, a single water molecule is bound behind each subunit of the selectivity filter. The final inactivation step is accompanied by the binding of two additional water molecules, leading to a characteristic configuration with three water molecules bound behind the constricted selectivity filter (***Ostmeyer et al., 2013***). These waters have been described to go through a gate formed by the Y82 “lid” residue (***Ostmeyer et al., 2013***; ***Cuello et al., 2017***).

The inactivation process has also been shown to be modulated by anionic lipids (***Alvis et al., 2003***; ***Demmers et al., 2003***; *Marius et al., 2008*; *Weingarth et al., 2013*; *Poveda et al., 2019*; *Zhang et al., 2021*; *Westerlund et al., 2020*). Mutagenesis experiments show that removing the co-purifying PG lipids bound between KcsA intersubunit pockets prevents inactivation, hightlighting their potential role in stabilizing the open state, or preventing entry into the inactivated one (*Poveda et al., 2019*). Several experimental techniques combined with MD simulations suggest that the inactivation mechanism is determined by the interaction between these bound PG-lipids, their anchoring residues (R89 and R64) and the inactivation-determining residues known as the “inactivation triad” (W67, E71 and D80)(*Cordero-Morales et al., 2011*; *Pless et al., 2013*; *Poveda et al., 2019*).

Molecular dynamics (MD) simulations are a powerful source of mechanistic information on the atomic level and, as such, many insights about ion channels (***Flood et al., 2019***; ***Lindahl and Sansom, 2008***; ***Carnevale et al., 2021***), including KcsA (***Poveda et al., 2019***; ***Li et al., 2018***; ***Furini and Domene, 2009***; ***Kopec et al., 2018***; ***Oakes et al., 2020***; ***Pérez-Conesa et al., 2021***; ***Westerlund et al., 2020***), have been obtained with this technique. One of the key modeling choices when using MD simulation is the choice of force field that describes the interactions between particles being simulated. For KcsA, this choice is crucial since the selectivity filter’s behaviour is remarkably force field-dependent (***Kopec et al., 2018***; ***Furini and Domene, 2020***). A recent study thoroughly compared the differences observed in the system when using either the CHARMM or AMBER force fields without concluding which best reproduced experimental findings (***Furini and Domene, 2020***). This dissimilarity suggests that the free energy surfaces that the system navigates may differ depending on the force field used to describe the system.

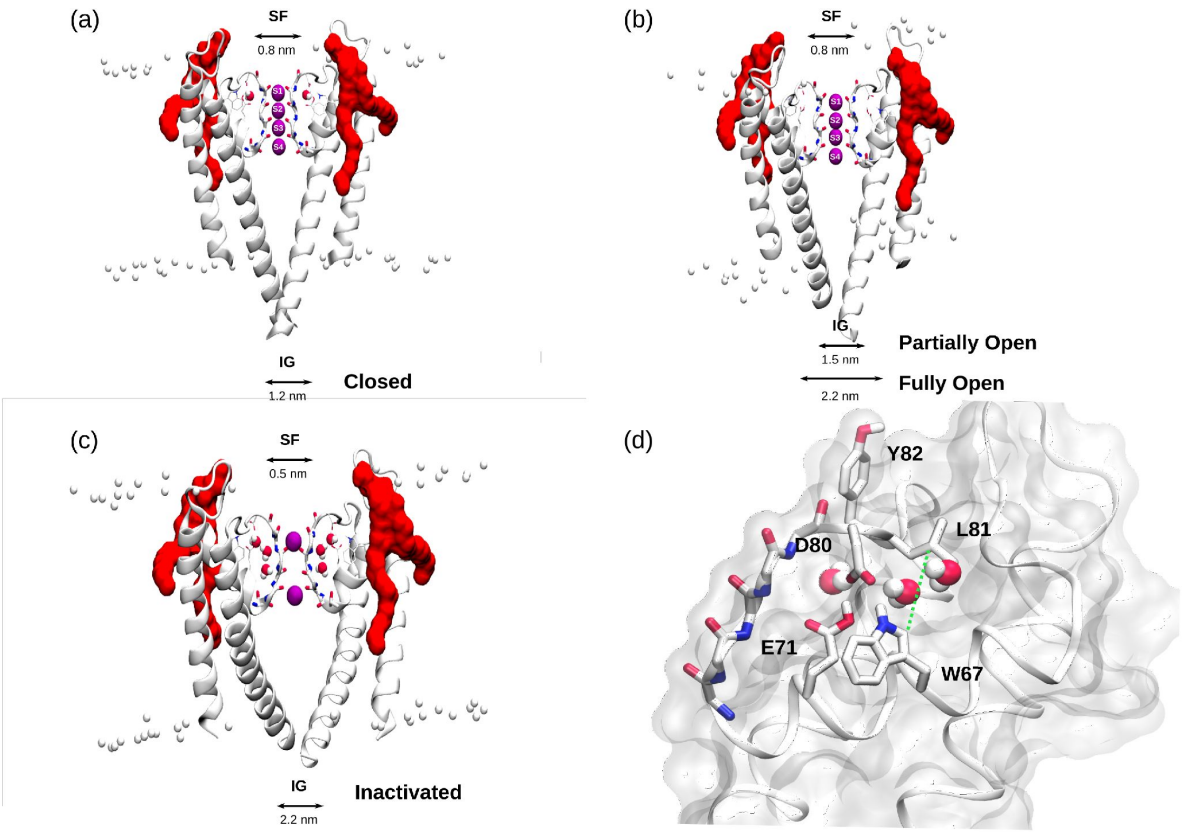

Figure 1.

Structure of two opposing subunits of the KcsA tetramer representing the closed state (a), the partially open and fully open states (b) and, the inactivated state (c). Potassium cations are represented by purple spheres, membrane lipid headgroups by white spheres, and bound DOPG lipids by their molecular surface in red. The typical values for their inner gate (IG) and selectivity filter (SF) openings are shown below each snapshot. (d) Representative MD snapshot of the pathway taken by water molecules before the final step of inactivation. This pathway passes between L81 and W67 (green dashed line) allowing for two additional water molecules to be buried behind the selectivity filter.

Estimating the free energy surface of processes as slow as KcsA inactivation, requires enhanced sampling MD simulations. Although there have been a few studies of selectivity filter constriction and ion permeation using enhanced sampling simulations (**Allen et al., 2004**; **Fowler et al., 2013**; **Li et al., 2018**; **Oakes et al., 2020**; **Furini and Domene, 2009**), a simulation study of the full inactivation path, emcompassing allosteric signal transmission between the two gates, is lacking.

Having an effective method to obtain the free energy surface of inactivation would allow studying the energetic impact of introducing perturbations in the system, such as single point mutations, or removing co-purifying PG-lipids. It is also of particular interest to understand whether the fully open state (PDB-ID 5VK6, captured using mutations to stabilize this specific conformation) is physiologically relevant, given that the partially open state (PDB-ID 3FB5) was recently shown to be the dominant state in activating conditions (**Pérez-Conesa et al., 2021**) in ssNMR experiments. Indeed, simulations based on the fully open state show spontaneous constriction of the selectivity filter(**Li et al., 2018**). Strikingly, however, constriction is observed only if the CHARMM force field is used, and no such events are observed over MD simulation timescales if the AMBER force field is used instead(**Furini and Domene, 2020**). All this begs the question: is the fully open state construct (PDB-ID 5VK6) a pre-inactivated transition state-like structure rather than a truly metastable state?

Building on previous characterization of the conformational ensembles of membrane proteins (Lev et al., 2017a; **Fleetwood et al., 2019**, 2021; **McComas et al., 2022**), in this work, we use the string method with swarms of trajectories (**Pan et al., 2008**) to obtain the full inactivation pathway free energy surface. Based on these simulations, we propose a potential role for residue L81 in opening a gateway for water molecules to enter behind the selectivity filter. We also contrast the free energy landscapes obtained using two different force fields, CHRAMM and AMBER. Finally, we investigate the role of co-purifying lipids by computing free energy surfaces with the bound lipids removed from their binding sites. We conclude by postulating a new inactivation mechanism, excluding the fully open state, observed using the CHARMM force field that could potentially be further supported or disproven by experimenting with an L81A construct.

Methods

System Preparation

KcsA coordinates were prepared using CHARMM-GUI (**Jo et al., 2017**) in the closed state. Residues 25–121 of the X-ray diffraction closed state structure (PDB-ID 5VKH (**Cuello et al., 2017**)) were used for consistency with our previous work. The selectivity filter was prepared fully loaded with potassium and one buried crystallization water behind each subunit's selectivity filter was included. All termini were NME- and ACE-capped and residues H25, E71, E118 and E120 were protonated following NMR data in activating conditions (**Pérez-Conesa et al., 2021**). Mutations in the experimental construct (Y82A, L90C and F103A) were reverted using PYMOL (**Lill and Danielson, 2011**). The protein was embedded in a 3:1 DOPE:DOPG membrane bilayer and surrounded by a 50mM KCl and 50mM NaCl solution including ~90 TIP3P rigid water molecules per lipid and a total of 150 lipids. The co-purifying bound PG lipids found between subunits were reconstructed as DOPG molecules following the partial coordinates of the experimental construct. Two starting coordinates were prepared one with the co-purifying lipids bound (LB) and another without these lipids (noLB). The lipid bound system was simulated using AMBER14SB+SLIPID16 and CHARMM36 (**Maier et al., 2015**; **Jämbeck and Lyubartsev, 2012**, **2013**; **Huang and MacKerell, 2013**) and the lipid unbound system only with AMBER14SB producing a set of three simulation conditions: LB-AMBER, noLB-AMBER and LB-CHARMM. CHARMM36 was used rather than the more recent CHARMM36m (**Huang et al., 2016**) to enable a direct comparison with Li et

al *Li et al. (2018)*. Nevertheless, our results are consistent with published data using CHARMM36m (*Kopec et al., 2018*; *Furini and Domene, 2020*). If unspecified, the system is assumed to have the PG lipids bound.

Molecular Dynamics Simulations

All molecular dynamics simulations were performed using GROMACS2020.5. The NPT ensemble was simulated using the Bussi thermostat (tau=1ps T=290K) and Parrinello-Rahman barostat (τ = 5 ps and P = 1 bar)(*Bussi et al., 2007*; *Parrinello and Rahman, 1981*). The temperature was chosen for compatibility with solid state NMR conditions and our previous work. The systems were equilibrated using an extended CHARMM-GUI protocol. Additional technical details can be found in the freely available input files (*https://github.com/delemottelab/KcsA_string_method_FES*).

String Method with Swarms of Trajectories

In order to sample the inactivation process, we used the string method with swarms of trajectories (*Pan et al., 2008*). Previous studies of pentameric ligand-gated ion channel activation (*Lev et al., 2017b*), GPCR activation (*Fleetwood et al., 2021*, *2019*) and sugar porters (*McComas et al., 2022*) have established this method as a useful tool for simulating and understanding protein conformational change. This method takes as input an approximate path connecting the initial state to the final state. Then, a set of initial structures along the path are taken as beads connected by a multidimensional string representing the structural transition. The multidimensional string is parametrized by a set of generalized coordinates known as collective variables (CVs) that describe the transition path and the slow degrees of freedom of the process. From each of the beads, a set of short “swarm” unbiased simulation replicas are launched. The average drift of the swarms in the string-CVs is calculated and used to update the position of the string. Then, equilibration simulations are launched from every bead restraining the CV values of the simulation to the new string iteration thus updating the coordinates of the beads to the new string iteration. This process is repeated until the string converges and oscillates around a fixed path in CV-space. This path corresponds to a minimum free energy pathconnecting the starting and final states. Many additional iterations are run in order to intensively sample the minimum free energy path for analysis.

To obtain the initial string, a steered simulation was performed starting from the equilibrated closed state (PDB-ID 5VKH), to the partially open state X-Ray coordinates (PDB-ID 3FB5), to the fully open state (PDB-ID 5VK6) and finally to the inactivated state (PDB-ID 5VKE). A harmonic potential was applied on a set of 60 steering-CVs (Table 1) moving the target CV value at a constant speed to force the channel to go through the mentioned conformational states in a total simulation time of ~500ns. The speed of steering was decreased in the final stages to allow the inactivation waters to enter the cavities behind the selectivity filter. The steering CVs were determined by structure comparison and bibliographical information of the system. For all steering simulations, unbiased simulations from the final coordinates were launched to check if the final state CVs remained stable and the system did not return to a fully-open-like state.

KcsA inactivation encompasses both rigid body motions such as the opening of the inner gate helical bundle and residue level motions such as the constriction of the selectivity filter, the motion of pore helix residues to stabilize it and accommodate the two additional buried water molecules per subunit. Thus to parametrize the string we used 36 interatomic distances, 11 of which are not symmetry related CVs. We chose: 18 CVs of TM2 cross- and adjacent-subunit distances to model inner gate opening, 8 CVs connecting allosteric contacts between the water cavity region and the SF (*Li et al., 2018*) that transmit the allosteric signal from the inner gate to the selectivity filter and 10 CVs related to the constriction of the SF. These CVs are a subset of the steering CVs and a result of filtering steering CVs that were unimportant in preliminary string simulation trials. The set of 36 CVs chosen to parametrize the string can be found in Table 2.

We observed in preliminary steering simulations of the CHARMM system that going from the fully open state (PDB-ID 5VK6) to the inactivated state (PDB-ID 5VKE), the contact between the sidechains of L81 and W67 spontaneously broke, in absence of any external bias explicitly acting on the distance between these two residues. This opened a gateway for two water molecules to enter the cavity behind the selectivity filter, eventually resulting in the obtention of the inactivated state with three buried waters per subunit, and an intact L81-W67 contact (***Figure 1e***). Subsequently adding this contact distance to the steering CV set promoted water penetration in all simulation conditions. In contrast, if this CV was not used during steering, water penetration was not observed until the spontaneous breaking of the mentioned contact at a significantly longer timescales, if this event even happened at all. We thus elected to include the breaking and reformation of this contact during the final inactivation step in our initial steering simulation, and included the distance between this residue pair as a string CVs.

The string method with swarms of trajectories was run using 18-bead strings obtained from the steering simulations fixing the endpoint beads. At each iteration, for every bead, a 100ps restrained simulation was performed and from each final snapshot, 32 10ps-swarms were launched to calculate the average drift of the strings. A total of ~800 iterations were run for minimum free energy path sampling after string convergence which occurred at 100 to 300 iterations. The convergence of the string equilibrium positions was evaluated with the time evolution of the beads and the root mean squared deviation of the string with respect to the initial string (***Figure 2—figure Supplement 1*** and ***Figure 2—figure Supplement 2***). The string simulations were performed using our own string method with swarms of trajectories python package which is freely available online (*https://github.com/delemottelab/string-method-swarms-trajectories*).

Free Energy Surface Calculation

Free energy surfaces were calculated using reweighted kernel density estimations of the probability distribution of CVs calculated per swarm trajectory snapshot. The weights of each swarm snapshot were obtained using a reversible maximum likelihood Markov State Model (MSM) with the deeptime python library (Hoffmann et al., 2021). The MSM was parametrized using states obtained from k-means clustering of a TICA dimensionality reduction of the string-CVs of the swarm trajectories. It is worth noting that since weights are assigned to the particular trajectory snapshot, the reweighted free energy surface can be projected to non-string CVs. Considering this, in order to have a more interpretable view of the path energetics, a one-dimensional projection of the free energy surface was also calculated. The CV chosen to describe the inactivation path is the progression along the converged path from the string simulations, s_{path}, being ~0 in the closed state and ~1 in the inactivated state. This path CV is calculated according to Braduardi's definition (***Branduardi et al., 2007***) and using as the converged path the average of the last 25 strings generated. This CV indeed represents correctly the progression along inactivation as can be seen in the overlay of the average path-CV value with the IG vs SF projected free energy surface (***Figure 2—figure Supplement 3***). Additional details of the MSM and free energy surface calculation can be found in the following repository (*https://github.com/delemottelab/KcsA_string_method_FES*.).

200ns long unbiased molecular dynamics started from the different free energy basins were started. These simulations have the expected stability based on their starting values (***Figure 2—figure Supplement 5***). This is a good quality test to check the correct estimation of the general features of the free energy surface.

The statistical errors of the free energy surface by combining blocking decorrelation analysis (***Flyvbjerg and Petersen, 1989***) and bootstrapping (***Hub et al., 2010***) (***Figure 2—figure Supplement 4***). The swarm data is divided into n blocks for n = 2, 4, 8, 16, 32 and 150 bootstraps are done on the blocks. The set of bootstraps for a given n is used to generate a distribution of free

energy surface. The error is then calculated as the standard deviation of this free energy surface distribution. n is chosen such that the average error over the free energy surface is maximized as a consequence of the time-decorrelation between the data of the blocks.

Results

Free energy surfaces reveal force field-dependent inactivation mechanisms

From the string method with swarms of trajectories, we obtained projections of the inactivation free energy surfaces onto the inner gate distance (IG, average cross-subunit distance between the CA of T112) and the selectivity filter distance (SF, average cross-subunit distance between the CA of G77 residues) (***Figure 2a-b***).

The free energy surface obtained using the AMBER force field (***Figure 2a***) shows an inactivation path which follows the canonical structural path inferred from X-ray crystallography data (***Doyle et al., 1998***; ***Cuello et al., 2010a,b***, ***2017***): closed state, partially open state, fully open state and inactivated state. In addition, the IG and SF of these states take very similar values to those of the crystal structure constructs, with the exception of a ~1 Å widening of the SF with respect to most unconstricted SF X-ray structures in the conductive states (PDB-IDs 1K4C, 5VKH, 3FB6 and 5VK6). The impact of the force field choice on the free energy surface of the systems is very strong. The CHARMM simulation explores a different minimum free energy path (***Figure 2***b). For CHARMM, the SF filter opening for the closed and partially open states is smaller than in AMBER simulations, similar to the XRD values of 0.8nm. This narrowing could rationalize the lower conductance obtained using the CHARMM force field (***Furini and Domene, 2020***). In addition, fully open-like IG distances lie outside of the minimum free energy path. In other words, using this force field, the only open state along the lowest free energy inactivation path is the partially open state. The partially open state to inactive state transition shows a correlated closing of the SF and opening of the IG, in contrast to the AMBER case where the SF constricts at a constant fully-open IG value. Additionally, the free energy barriers using CHARMM are substantially lower than using AMBER.

Our previous investigation combining solid-state NMR and MD simulations had inferred that a partially open state was more energetically favorable than a fully open state under activating conditions(***Pérez-Conesa et al., 2021***). This experimental evidence is in agreement with the lower FE basins corresponding to the partially open state obtained using both the AMBER and the CHARMM force field. Furthermore, the fact that our systems prepared with the protonation states and salt concentration used in activating conditions solid-state NMR experiments show partially open states thermodynamically accessible from the resting state exemplifies the quantitative agreement of the method with independently obtained experimental data.

The 1-D free energy surface of the path-CV, s_{path}, which measures the progression along the reaction path, shows profiles with comparable features using both force fields (***Figure 2***c-d). The lowest basin is the closed state (s_{path} ~ 0.2). The shallow basins of the open state or open states, of higher free energy, are then explored (s_{path} ~ 0.4 and s_{path} ~ 0.6 for AMBER and s_{path} ~ 0.35 CHARMM). Finally, there is a substantial free energy barrier leading to the highest free energy basin (s_{path} ~ 0.9), corresponding to the inactivated state, consistent with our simulations being run under activating conditions. Energetically speaking, the main effect of the force field choice is the increase in the barrier and difference in free energy between the closed state and the inactivated state. In particular, the barrier height and difference in free energy of inactivation are ~14kT and ~ 13kT for AMBER and ~6kT and ~ 4kT for CHARMM, respectively. Given that our simulations were conducted under activating conditions, we had expected the open states to be more populated than the closed ones. Simulations carried out at higher pH may be able to resolve this inconsistency.

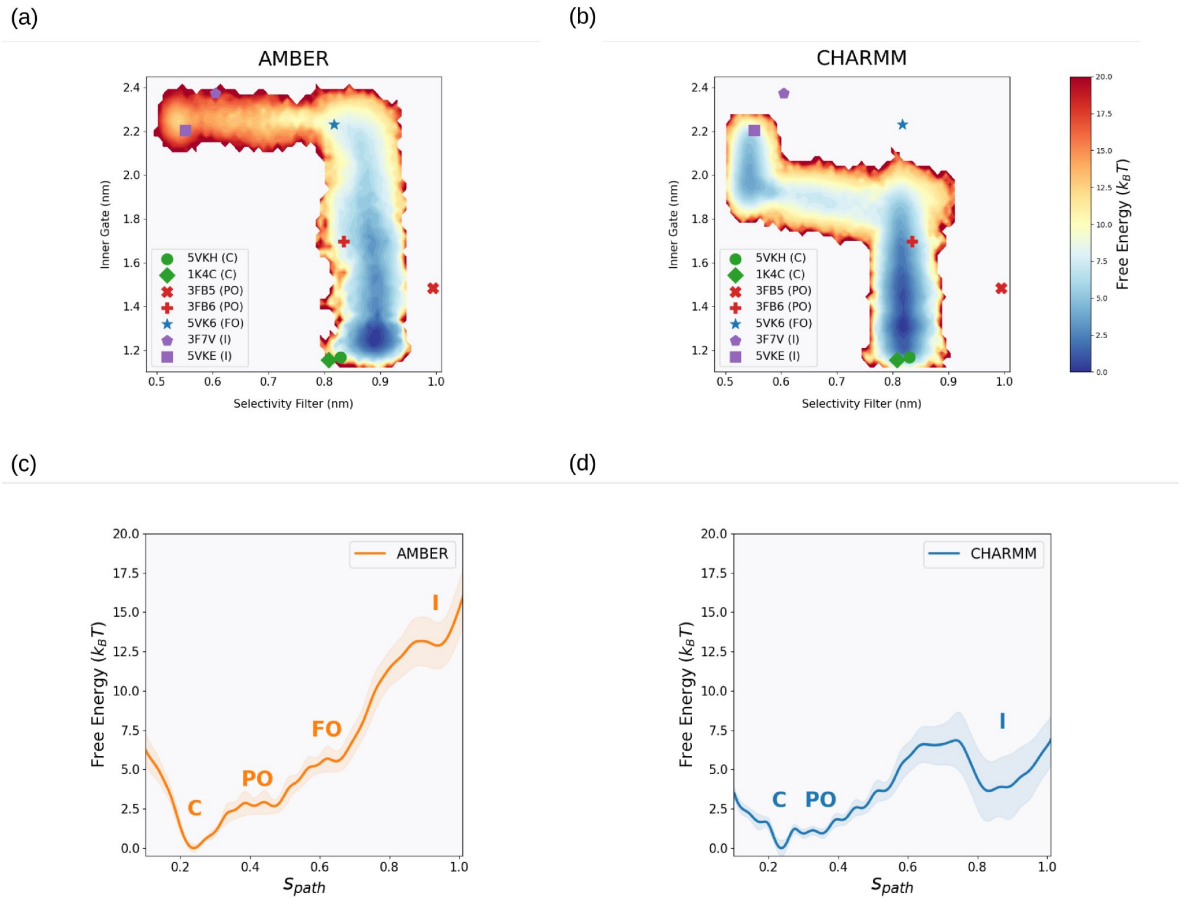

Figure 2.

Reweighted free energy surfaces calculated from the string method with swarms of trajectories. 2D free energy surfaces projected on the inner gate distance (IG, average cross-subunit distance between the CA of T112) and the selectivity filter distance (SF, average cross-subunit distance between the CA of G77 residues) of the systems using (a) AMBER and (b) CHARMM. 1D free energy surfaces projected on the path cv ($spath$) of the systems using (c) AMBER and (d) CHARMM with labels denoting the state of the basin: closed (C), partially open (PO), fully open (FO) and inactivated (I). The errors associated with the 2D-free energy surface can be found in **Figure 2—figure Supplement 4**

Figure 2—figure supplement 1. Evolution of the string beads over the string method iteration (averaged over blocks of 25 iterations) and projected on the inner gate distance (IG, average cross-subunit distance between the CA of T112) and the selectivity filter distance (SF, average cross-subunit distance between the CA of G77 residues). The initial string is represented as a black dotted line. The inset plots the first ten iterations without averaging. The systems represented are (a) LB-AMBER, (b) LB-CHARMM and (c) noLB-AMBER.

Figure 2—figure supplement 2. Evolution of the root mean squared deviation from the initial string averaged over all beads. The systems represented are LB-AMBER (orange), LB-CHARMM (blue) and noLB-AMBER (red).

Figure 2—figure supplement 3. The weighted average value of $spath$ projected 2D-free energy surface projected on the IG and SF. The systems represented are (a) LB-AMBER, (b) LB-CHARMM and (c) noLB-AMBER.

Figure 2—figure supplement 4. Estimation of the uncertaintly associated with the 2D-free energy surface projected on the IG and SF (see Methods). The systems represented are (a) LB-AMBER, (b) LB-CHARMM and (c) noLB-AMBER.

Figure 2—figure supplement 5. IG and SF projections of 200 ns MD trajectories started from representatives of different states of the inactivation cycle onto corresponding free energy surface. The starting structure is represented as a triangle. The systems represented are (a) LB-AMBER, (b) LB-CHARMM and (c) noLB-AMBER.

Free energy landscapes offer insights into atomistic-resolution mechanistic details

Free energy surface projection along the path-CV and another CV of interest allows studying how the CV of interest evolves with the inactivation process. One can thus observe correlations between the advancement in inactivation and the CV of interest, switch-like events, or lack of correlation. A set of these projections were calculated using as CVs of interest potential allosteric communication contacts, secondary structure movements, rotamer changes, etc. (***Figure 3***, ***Figure 3—figure Supplement 1***, ***Figure 3—figure Supplement 2*** and ***Figure 3—figure Supplement 3***)

In general, two types of behaviours of meaningful CVs of interest were observed: correlational and switch-like. In the first category, the minimum free energy path of the CV of interest changes linearly with the path-CV. In the second category, the FE path of the CV of interest switcheds abruptly along the path-CV. We first focus our analysis on the AMBER free energy surface, before then contrasting the differences when working with the CHARMM force field.

There is a clear correlation between path-CV and the opening of the inner gate except for the final step linking the fully open state and the inactivated one, during which it the inner gate opening remains constant (***Figure 3a***). The same behavior is observed for the contraction of the T74-F103 distance (***Figure 3b***) and the expansion of the T74-I100 distance (***Figure 3—figure Supplement 1a***), both of which are considered important contacts for the transmission of the IG signal to the SF, and (***Cuello et al., 2010a***; ***Labro et al., 2018***; ***Li et al., 2018***).

The rotameric state of E71 is a clear marker of inactivation given that for the three water molecules to be accommodated behind the SF and to form four hydrogen bonds each, it must undergo a rotameric switch (***Li et al., 2018***; ***Ostmeyer et al., 2013***). Its projected free energy surface presents a conformational distribution where E71 χ_1 remains at 50-100˚ in closed and open states before switching to 360˚ during the final inactivation step (***Figure 3c***). The conformation of F103, which is known to move away from the water cavity below the SF during the inactivation process to due to the breaking of the hydrophobic contact with I100 ((***Li et al., 2018***)), displays a switch-like behavior (***Figure 3d***).

Previous experimental and computational studies have pointed out the importance of R89 and R64 interactions since they interact with the key inactivation residue D80 and also anchor the copurifying lipid, thus mediating the effect of lipid binding on inactivation (***Poveda et al., 2019***). In our simulation, we were able to point out a clear switch-like behavior for the R64-D80 distance (***Figure 3e***). The distance between the sidechains shrinks by 0.4 nm during the final step of inactivation. This highlights the involvement of R64, and indirectly of the anionic copurifying lipid in the process. We also found little to no correlation between the R89-D80 distance and the progression along the path (***Figure 3—figure Supplement 1b***) and the phosphate group of the lipids with either arginine (***Figure 3—figure Supplement 1c-d***, ***Figure 3—figure Supplement 2i-j***, ***Figure 3—figure Supplement 3i-j***,).

The 2D path-CV projections of the simulations conducted using the CHARMM force field generally follow similar patterns to those using AMBER (***Figure 3—figure Supplement 1***, ***Figure 3—figure Supplement 2*** and ***Figure 3—figure Supplement 3***). The main difference is that, for AMBER, more CVs of interest tend to adopt a switch-like behavior, while using CHARMM results in correlation-like behaviors. This follows from the nature of the last step of inactivation: using AMBER, the selectivity filter constricts at constant inner gate opening while this process is concerted in CHARMM.

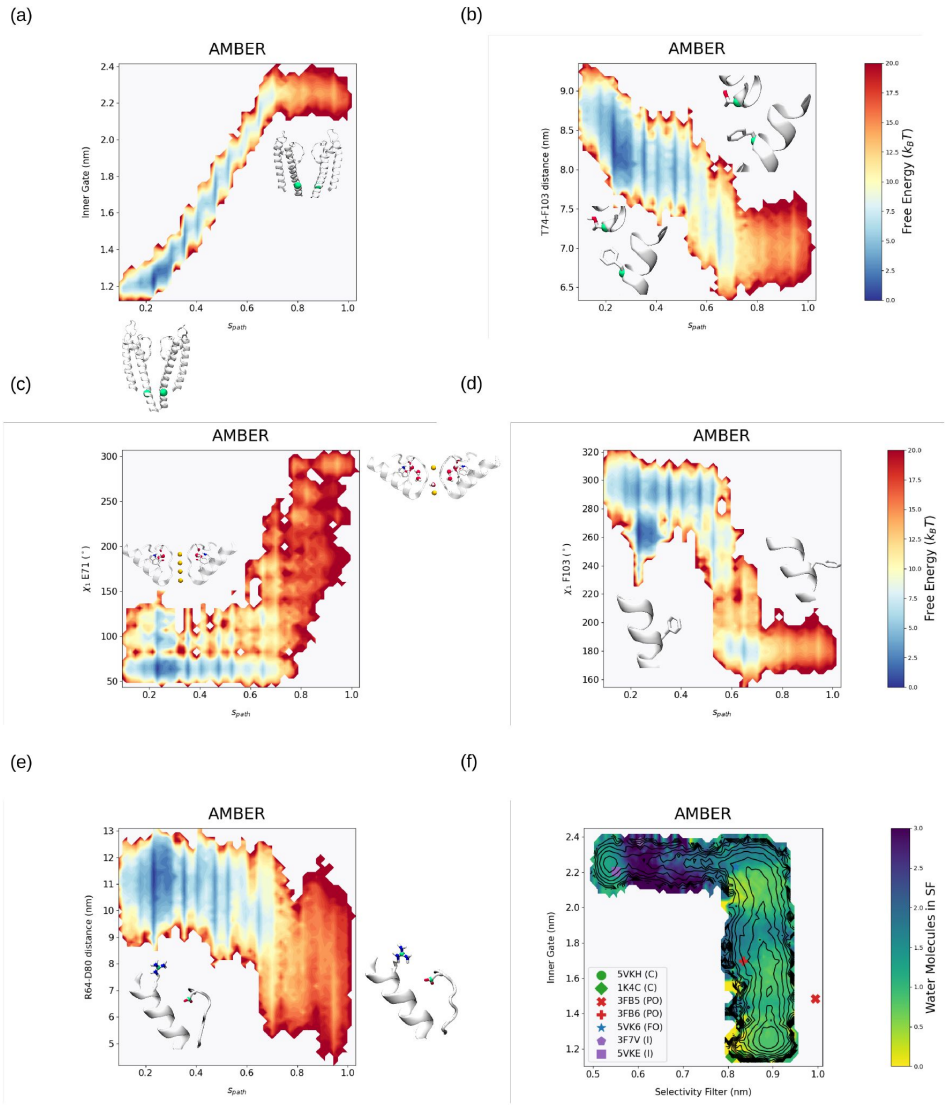

Figure 3.

Reweighted free energy surfaces calculated from the string method with swarms of trajectories of the AMBER with lipids bound system. 2D free energy surfaces projected on the path cv ($spath$) and an additional CV of interest. These CVs of interest are: (a) Inner gate distance, (b) T74 CA - F103 CA distance, (c) E71 χ_1 Janin angle, (d) F103 χ_1 Janin angle and (e) R64 CZ - D80 CG distance. (f) Projected weighted average number of water molecules inside the selectivity filter (sites S1-S4) on the free energy surface of the AMBER lipid bound system.

Figure 3—figure supplement 1. Reweighted free energy surfaces calculated from the string method with swarms of trajectories of the AMBER with lipids bound system. 2D free energy surfaces projected on the path cv ($spath$) and an additional CV of interest. These CVs of interest are: (a) T74 CA - I100 CA distance and (b) R89 CZ - D80 CG distance (c) Copurifying DOPG P - R64 CZ distance (d) Copurifying DOPG P - R89 CZ distance.

Figure 3—figure supplement 2. Reweighted free energy surfaces calculated from the string method with swarms of trajectories of the CHARMM with lipids bound system. 2D free energy surfaces projected on the path cv ($spath$) and an additional CV of interest. These CVs of interest are: (a) Inner gate distance, (b) T74 CA - F103 CA distance, (c) E71 χ_1 Janin angle, (d) F103 χ_1 Janin angle, (e) R64 CZ - D80 CG distance, (g) T74 CA - I100 CA distance and (h) R89 CZ - D80 CG distance. (f) Projected weighted average number of water molecules inside the selectivity filter (sites S1-S4) on the free energy surface of the CHARMM lipid bound system (i) Copurifying DOPG P - R64 CZ distance (j) Copurifying DOPG P - R89 CZ distance.

Figure 3—figure supplement 3. Reweighted free energy surfaces calculated from the string method with swarms of trajectories of the AMBER without lipids bound system. 2D free energy surfaces projected on the path cv ($spath$) and an additional CV of interest. These CVs of interes9toafre1:9(a) Inner gate distance, (b) T74 CA - F103 CA distance, (c) E71 χ_1 Janin angle, (d) F103 χ_1 Janin angle, (e) R64 CZ - D80 CG distance, (g) T74 CA - I100 CA distance and (h) R89 CZ - D80 CG distance. (f) Projected weighted average number of water molecules inside the selectivity filter (sites S1-S4) on the free energy surface of the AMBER without lipid bound system (i) Copurifying DOPG P - R64 CZ distance (j) Copurifying DOPG P - R89 CZ

To characterize the role played by the selectivity filter-bound water molecules in inactivation; we report the average number of water molecules (***Figure 3f***) in the SF along the inactivation path. The number of water molecules in the SF sites was found to be 0.5-1.5 in closed and open states. A per-site analysis of SF water occupation revealed that this corresponds mostly to water binding in S1, while sites S2 and S3 are fully loaded with K+ ions (***Figure 3—figure Supplement 8***). S4, on the other hand, transitions from being K+ bound to water bound as the channel proceeds to more and more open states. In the transition regions before the final inactivation step of SF constriction, there is an increase in average water occupation to 2-2.5 water molecules. These water molecules are localized in the S1, S2 and/or S4 sites . In the inactivated state, water mainly occupies S2. In contrast, for the CHARMM force field, the closed and conductive states are devoid of water in the selectivity filter, and S1, S2 and S4 are filled with K+ ions (***Figure 3—figure Supplement 2f***, ***Figure 3—figure Supplement 9***). In the transition region towards inactivation, the ion in S2 becomes replaced by water and S2 and S3 become hydrated in the inactivated state.

Our initial string featured the breaking and reforming of the L81-W67 contact during the final step of inactivation, allowing water molecules to bind behind the SF. This relied on the spontaneous observation of this phenomenon in the initial steering simulations (see methods). Studying the L81- W67 distance as a function of the progression of the equilibration of the string in each subunit of the channel, we can observe that, for the AMBER force field, this mechanism remains in a single one subunit(***Figure 3—figure Supplement 4***). In contrast, for the CHARMM force field, this path is followed by three of the four subunits (***Figure 3—figure Supplement 5***). This may show that this novel mechanism is energetically accessible to both force fields but only thermodynamically dominant when using the CHARMM force field. Instead, in both force fields, in the subunits where water does not enter via the L81-W67 pathway, the W67-D80 hydrogen breaks instead, leading to water penetration via this path. Surprisingly, we found no evidence of water penetration via the opening of the Y82 residue, in contrast to its purported role as a lid residue (***Ostmeyer et al., 2013***).

Unbinding of copurifying PG-lipids stabilizes the open states

To study the effect of bound copurifying lipids on the inactivation mechanism, we prepared systems without any lipids anchored in the binding sites (noLB-AMBER simulations). During equilibration, steering and string simulations, however, randomly positioned DOPG lipids near the protein spontaneously bound or partially bound to the intersubunit binding sites. This produced a set of heterogeneous occupation states of the binding sites along the string. Nevertheless, the number of bound lipids remained lower than in the fully bound simulations, with an occupancy around one to two out of four.

Despite this, there is a clear impact of the low lipid binding site occupancy in the inactivation landscape (***Figure 4-b***): the partially open state is significantly stabilized in the absence of lipids (***Figure 4c-d***) and the fully open basin appears unstable as unbiased MD simulations initiated in this basin spontaneously convert to partially open states (***Figure 2—figure Supplement 5***). This suggests that stabilization of the partially open state by the removal of bound lipids can explain the increase in open probability and reduced inactivation of the channel upon mutation of the PG-anchoring residues (***Poveda et al., 2019***).

Discussion and conclusion

Molecular dynamics simulations offer atomistic insights into the function of biomolecules and can complement other experimental techniques advantageously. One of their main drawbacks is that the timescales that they allow to sample are generally much shorter than phenomena of physiological or even biophysical relevance. Enhanced sampling MD simulations have emerged as a way to expand the scope of MD simulations, while keeping an atomistic level of resolution. Many

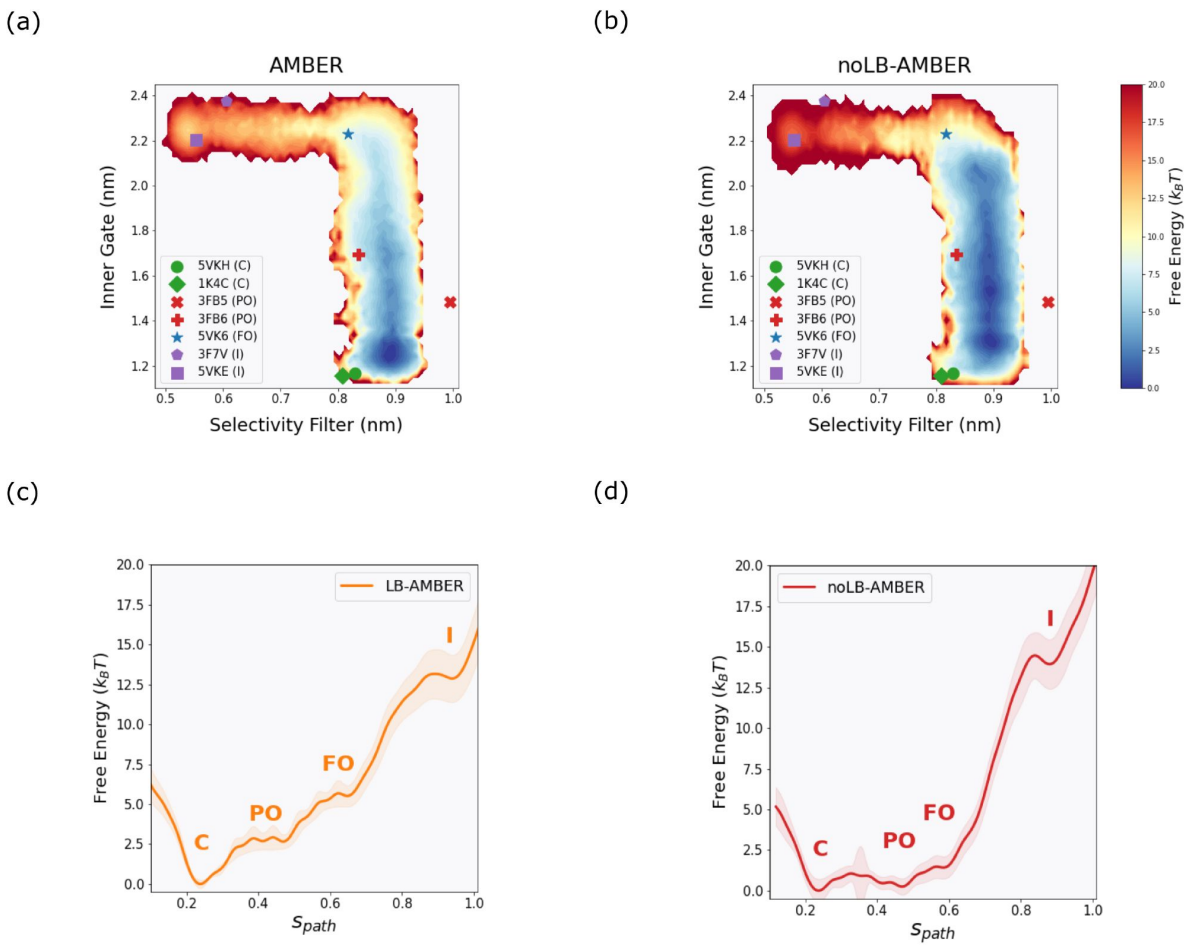

Figure 4.

Reweighted free energy surfaces calculated from the string method with swarms of trajectories. 2D free energy surfaces projected on the inner gate distance (IG, average cross-subunit distance between the CA of T112) and the selectivity filter distance (SF, average cross-subunit distance between the CA of G77 residues) of the system with (a) PG-lipids bound and (b) no PG-lipids bound using the AMBER force field. 1D free energy surfaces projected on the path cv ($spath$) of the system with (a) PG-lipids bound and (b) no PG-lipids bound using the AMBER force field with labels denoting the state of the basin: closed (C), partially open (PO), fully open (FO) and inactivated (I).

such techniques require a reduction of the dimensionality of the problem via an identification of a low number of degrees of freedom, or collective variables, that can separate different functional states of the system. Such dimensionality reduction is non trivial, and may not even be possible for all systems and processes. We have thus chosen a variant of the string method, called the string method with swarms of trajectories, in which a single minimum free energy paths linking conformational states is optimized. This method doesn't require a dimensionality reduction as drastic as other methods, since the minimum free energy path can be optimized in high-dimension. The resulting conformational ensemble can later be projected along any collective variable interest, resulting in low-dimension free energy landscapes that can be interpreted.

Here, we have calculated the inactivation free energy surface of KcsA. These landscapes, calculated under activatory (low pH and high salt concentration) conditions, show stable closed and partially open states. The fully open state appears less stable. The pathway to inactivation features a relatively high free energy barrier. Enhanced sampling enables us to characterize the entire inactivation path under activating conditions, including the inactivated state, even if this state is not energetically favorable and would only be seldom visited using regular MD simulations. Conformational free energy landscapes are typically obtained aggregating several hundreds of microseconds of MD simulations data. Using this methodology represents a substantial computational gain, such that this type of study can be extended to study the effect of mutations, changes in pH or ion concentration.

Another major issue one is faced when using MD simulations is the choice of a potential interaction energy function (or force field) that models the processes of interest with enough accuracy. In this case, contrasting the landscapes obtained using two popular force fields suggests diverging mechanisms for the most energetically favorable inactivation cycle of KcsA. Using AMBER suggests that the fully open state is the last metastable state before selectivity filter constriction (***Figure 5a***). In this case, the selectivity filter constraints at constant inner gate opening. In contrast, using CHARMM reveals that the partially open state is the final metastable state before selectivity filter constriction, the fully open state lying outside the minimum free energy path (***Figure 5b***). In this case, the selectivity filter constricts concertedly with an inner gate expansion. This mechanism defies the current canonical inactivation path of KcsA. Interestingly, this mechanism (***Figure 5b***) is obtained despite the initial string preparation assuming the canonical path (***Figure 5a***).

Molecular dynamics simulations started from the fully open state derived from the XRD structure with PDB-ID 5VK6 have been repeatedly observed to leads to selectivity filter constriction when the CHARMM force field is used (***Ostmeyer et al., 2013***; ***Li et al., 2018***; ***Furini and Domene, 2020***). This phenomenon is even observed for the constitutively conductive mutant E71A (***Furini and Domene, 2020***). In contrast, the AMBER force field does not lead to inactivation of the WT channel on the MD timescale (***Furini and Domene, 2020***). It has been argued that the extremely fast kinetics of this process in CHARMM simulations contrasts with its slower nature in experiments (seconds timescale) because this process represent fast SF switching instead of inactivation (***Jekhmane et al., 2019***). Others have argued that this is rather due to a bias of the force field towards the inactivated state (***Furini and Domene, 2020***). Our free energy surfaces paint a slightly more complex picture. For the CHARMM force field, states resembling 5VK6 would lie in shallow high-free basins outside the minimum free energy path. In this way, the force field does not bias towards inactivation directly but rather displays a different inactivation path excluding 5VK6-like structures. The less favorable pathway passing through the fully activated state presumably features a spontaneous downhill process linking the fully open and the inactive state. The AMBER force field, on the other hand, does incorporate a fully-open state in its mean free energy path. These two force fields differ in several ways, and precisely pinpointing the reason(s) for which these different pathways are observed would require a separate study. Likely candidates leading to different mechanisms are different ion-carbonyl and ion-water interaction strengths (***Kopec et al., 2018***; ***Furini and Domene, 2020***), as well as more recently highlighted

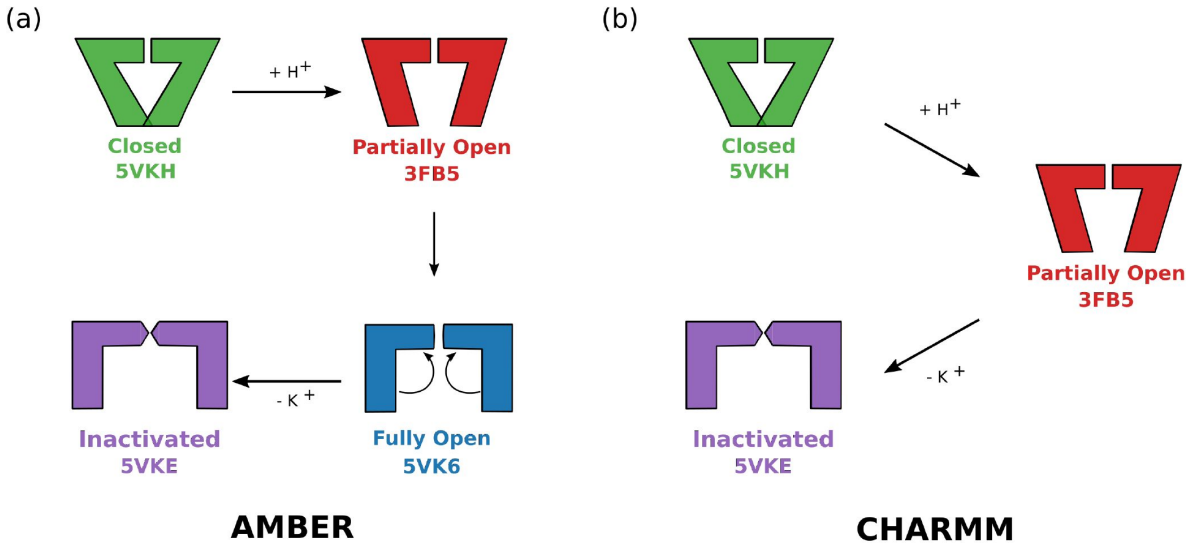

Figure 5.

Schematic depiction of the two possible inactivation mechanisms of KcsA as described by the minimum free energy paths obtained by the string method with swarms of trajectories for the AMBER (a) and CHARMM (b) force fields.

differences in the parametrization of glutamate charge and dihedral side chains (**Kopec et al., 2022**). Nevertheless, both force fields yield inactivation barriers that are orders of magnitude lower than what is expected from electrophysiology experiments (**Ostmeyer et al., 2013**) if we assume a transition state theory approximation of the kinetics (Equa-tion 1).

Different experimental evidence offer more support to one or the other mechanism we observe. The AMBER free energy surface follows the X-diffraction structures and displays a higher inactivation barrier. The CHARMM force field, on the other hand, results in landscapes in agreement with fact that the one of the dominant states in activating conditions is the partially open state, as revealed by a combination of ssNMR+MD.

The block of conduction during inactivation appears to result from pinching at the selectivity filter, which is triggered by water molecules entering the selectivity filter, and the cavities behind the TVGYG sequence. These phenomena appear to follow opening of the inner gate, which seems to allosterically trigger changes in the region surrounding the SF. The contact between the residue at the bottom of the selectivity filter, T74, and the hydrophobic residues on the pore lining residues I100 and F103 have previously been suggested to be important (**Cuello et al., 2010a**; **Labro et al., 2018**; **Li et al., 2018**). Interestingly, our landscape show that T74 and I100 gradually move away from one another along the opening pathway while T74 and F103 gradually move closer together. Interestingly, the sidechain of F103 keeps its upward orientation during the first opening steps of the inner gate, and abruptly undergoes a change to a horizontal conformation after passing through the partially open state, likely enabling a tighter contact between T74 and F103. The two force fields we used in this work are broadly consistent in this description. However, the last step towards the inactivated state happens at constant inner gate opening in AMBER while it happens as the gate further opens in CHARMM. All the degrees of freedom we have probed reveal a similar behavior with abrupt transitions in AMBER and more gradual ones in CHARMM.

Our simulations are consistent with selectivity filter pinching been triggered by the penetration of water molecules in the selectivity filter, as previously observed by different research groups (**Furini and Domene, 2020**; **Kopec et al., 2019**). While both force fields paint a different detailed mechanistic picture, they are broadly consistent in reporting that replacement of a K+ ion by a water molecule in S2 is a key step towards destabilization of the SF in its conductive conformation, in agreement with recent observations from ssNMR (**Rohaim et al., 2022**).

Y82 was first proposed to be the “lid” that had to open to allow the buried water molecules to enter the cavity behind the SF on the basis of unbiased MD simulations of the closed state using the CHARMM force field (**Ostmeyer et al., 2013**). This same observation in fully-open-like state simulations (**Li et al., 2018**) and the fact that the Y82A mutant displays fast inactivation solidified this hypothesis. Our simulations show that for the CHARMM force field, the fully-open like states lie outside the minimum free energy path potentially, making simulations initiated in this state of limited relevance. In our simulations, the sidechain χ_1 and χ_2 of Y82 show little correlation with the path-CV in nearly all subunits analyzed. Here, we instead find that water entry proceeds via a pathway that is opened thanks to the breaking of the L81-W67 or the D80-W67 contacts. An alternative explanation for the fast inactivation of the Y82A mutant could be that removing the bulky tyrosine sidechain facilitates the opening of a water pathway adjacent to this residue, possibly involving W67. Mutating L81 could potentially add clarifying evidence to this question. Indeed, our research suggests that the mutation would enhance inactivation by allowing water to enter behind the SF without needing to wait for the L81-W67 gateway to open. In addition, given the strong force field dependence of this phenomenon, this information could help in determining which force field better describes the system in general: since L81 pathway is correlated with the overall inactivation mechanism, investigating L81A could shed light on the question whether if the fully open state is a part of KcsA’s inactivation cycle. Indeed, if the L81A mutation conserves wildtype inactivation, L81 would most likely not be involved in the

mechanism suggesting that the AMBER mechanism is most likely. On the other hand, if L81A is a fast inactivator, this evidence would support the CHARMM mechanism which excludes the fully open-like states and highlights the importance of breaking the L81-W67 contact for water penetration.

To gain insights into the effect of bound POPG lipids on the inactivation mechanism, we have compared our original free energy surfaces, in which co-purifying lipids were indeed bound to the channel, with systems in which these lipids were removed. We observed that the removal of these lipid molecules stabilizes partially open states, potentially offering an explanation for the increased open probability observed in single-channel recordings of R64A and R89A mutants. These mutations are indeed proposed to lead to a destabilization of lipid binding. We could also observe that D80 and R64 come closer together as inactivation proceeds. When no lipids are bound, this stabilizing interaction appears less likely to form, which probably leads to a less likely destabilization of the interactions that keep the SF in a non-pinched, conductive, state.

KcsA has long been thought of as a prototype for K+ channel function. Recent evidence is however pointing towards the fact that its inactivation mechanism may be quite unique. Indeed, new structures of the fast inactivating W434F mutant show that the Drosophila Shaker channel likely inactivates via a different C-type inactivation mechanism, which involves widening of the upper part of the SF instead of pinching at the first Glycine residue (***Tan et al., 2022a***). This appears to be triggered by the destabilization of the network of interactions behind the selectivity filter (***Tan et al., 2022b***), triggered by the breaking of the D447-W434 (KcsA numbering D80-W67) contact following the mutation of W434 to Phe (***Pless et al., 2013***). This leads to a repositioning of the entire loop of residues that follow the TVGYG sequence, with a notable reorientation of D447 in a solution-facing position. A similar mechanism was described in structures of Kv1.3 (***Selvakumar et al., 2022***), of the Kv1.2 W362F mutant (***Reddi et al., 2022***), and could also be at play in K2P channels (***Lolicato et al., 2020***). In KcsA, on the other hand, this work agrees with previous suggestions that the breaking of D80-W67, when it occurs, does not lead to a major reorientation of the loop containing D80, but instead to the pinching of the SF stabilized by water molecules that were able to enter cavities via the pathway made accessible by the breakign of this contact.

A singularity in KcsA is the presence of an aspartic acid in position E71. This residue, found to be protonated by ssNMR, interacts with D80 and W67 (***Figure 1d***). We have found that E71 must adopt a different rotameric state to accommodate the water molecules bound to the back of the selectivity filter in the inactivated state. However, in our simulations, the orientation of the E71 side chain remains the same throughout the conformational change, namely E71 stays in an upward facing position even in the inactivated state. Other K+ channels generally feature a hydrophobic residue at this position. MthK, for example, contains a Val residue, V55. The presence of an aspartate residue in this position is thought to favor the stabilization of water molecules behing the selectivity filter. MD simulations of the V55E, engineered to mimic KcsA, reveal that this mutant appears to inactivate through a mechanism more similar to Shaker than to KcsA(***Kopec et al., 2022***), though SF carbonyl flipping is reminiscent of the behavior in KcsA(***Boiteux et al., 2020***; ***Kopec et al., 2022***). This is accompanied by a reorientation of E71 in a horizontal orientation, a phenomenon that is never observed in our study. We note, however, that MthK features a Tyr in place of W67, Y51, and the details of the interactions between residues is thus overall different in these channels, making transposing the mechanistic insights from this study to other channels non trivial.

Acknowledgements

S.P.-C. was supported by a postdoctoral scholarship of the Gustafsson foundation. L.D. would like to thank the support of Science for Life Laboratory, the Göran Gustafsson Foundation, and the Swedish Research Council (Grants No. VR-2018-04905, 2019-02433 and 2022-04305). Simulations

were performed on computational resources provided by the Swedish National Infrastructure for Computing (SNIC) at the PDC Centre for High Performance Computing (PDC-HPC). Additionally, the authors would like to thank Wojciech Kopec for the interesting discussions.

Data Availability

The data and code to reproduce this work can be found at *https://osf.io/snwbc/* and *https://github.com/delemottelab/KcsA_string_method_FES*. The python package to run the string method with swarms of trajectories is freely available at *https://github.com/delemottelab/string-method-swarms-trajectories*

Transition state theory for rate estimation

In the context of transition state theory the rate of a process, k is given by the Eyring equation:

$$k = \frac{\kappa k_B T}{h} \exp -\frac{\Delta G^{\dagger}}{k_B T} \quad (1)$$

Where κ is a correction factor that is equal to 1 if transition state theory is followed ideally, k_B is the Boltzmann constant, h is Planck's constant, T is the temperature and $\Delta G^{\dagger}$ is the reaction barrier. The inverse of k is related to the mean-life of the process.

Biased collective variables

Residue	Atom	Residue	Atom	Sub-units
77	CA	77	CA	AB, CD
77	CA	77	CA	AC, DB, AD, DA
104	CA	77	CA	AB, CD
108	CA	77	CA	AB, CD
112	CA	77	CA	AB, CD
103	CZ	74	CG2	AA, BB, CC, DD
100	CD	75	CG2	AA, BB, CC, DD
103	CZ	100	CD	AD, BD, BC, AC
114	CA	32	CA	AC, CB, BD, DA
32	CA	114	CA	CA, BC, DB, AD
118	CA	28	CA	AD, BD, BC, AC
107	OG1	101	OG1	AD, BD, BC, AC
67	NE1	80	CG	AA, BB, CC, DD
71	OE1	68	CA	AA, BB, CC, DD
71	OE1	78	HN	AA, BB, CC, DD
74	CA	79	CA	AA, BB, CC, DD
67	CD1	81	CG	AA, BB, CC, DD

Appendix 0—table 1.

Distance CVs used for the steering simulations. AB and CD subunits are opposing each other and AC, CB, BD and DA subunits are side by side in a clockwise fashion observing the channel from the intracellular side.

Residue	Atom	Residue	Atom	Sub-units
77	CA	77	CA	AB, CD
77	CA	77	CA	AC, DB, AD, DA
104	CA	77	CA	AB, CD
108	CA	77	CA	AB, CD
112	CA	77	CA	AB, CD
103	CZ	100	CD	AD, BD, BC, AC
114	CA	32	CA	AC, CB, BD, DA
32	CA	114	CA	CA, BC, DB, AD
118	CA	28	CA	AD, BD, BC, AC
107	OG1	101	OG1	AD, BD, BC, AC
67	CD1	81	CG	AA, BB, CC, DD

Appendix 0—table 2.

Distance CVs used for the string simulations. AB and CD subunits are opposing each other and AC, CB, BD and DA subunits are side by side in a clockwise fashion observing the channel from the intracellular side.

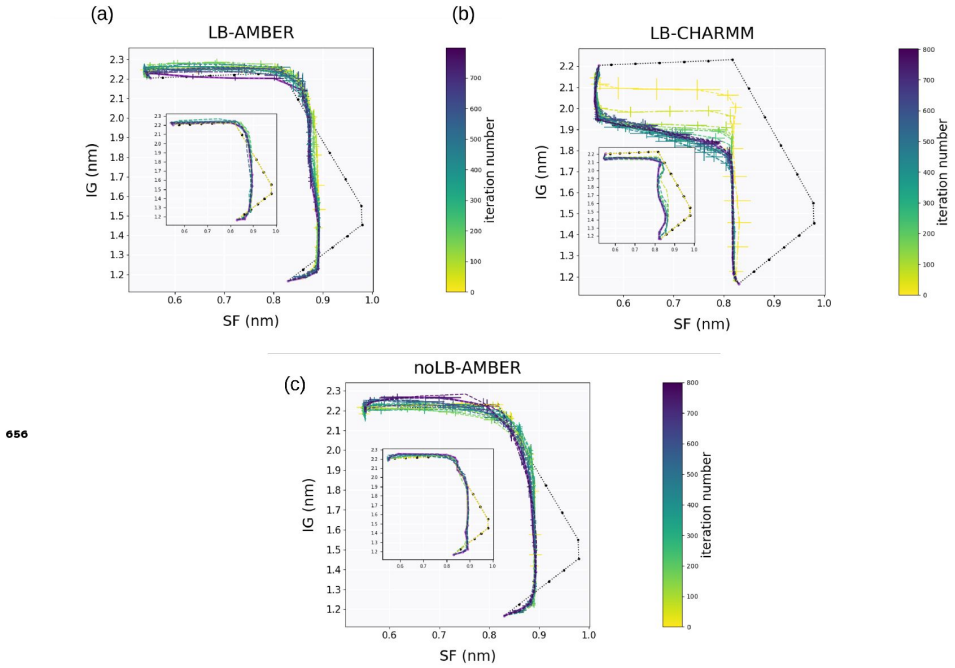

Figure 2—figure supplement 1.

Evolution of the string beads over the string method iteration (averaged over blocks of 25 iterations) and projected on the inner gate distance (IG, average cross-subunit distance between the CA of T112) and the selectivity filter distance (SF, average cross-subunit distance between the CA of G77 residues). The initial string is represented as a black dotted line. The inset plots the first ten iterations without averaging. The systems represented are (a) LB-AMBER, (b) LB-CHARMM and (c) noLB-AMBER.

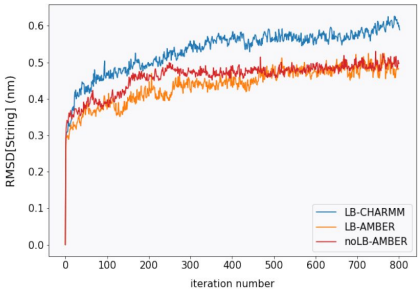

Figure 2—figure supplement 2.

Evolution of the root mean squared deviation from the initial string averaged over all beads. The systems represented are LB-AMBER (orange), LB-CHARMM (blue) and noLB-AMBER (red).

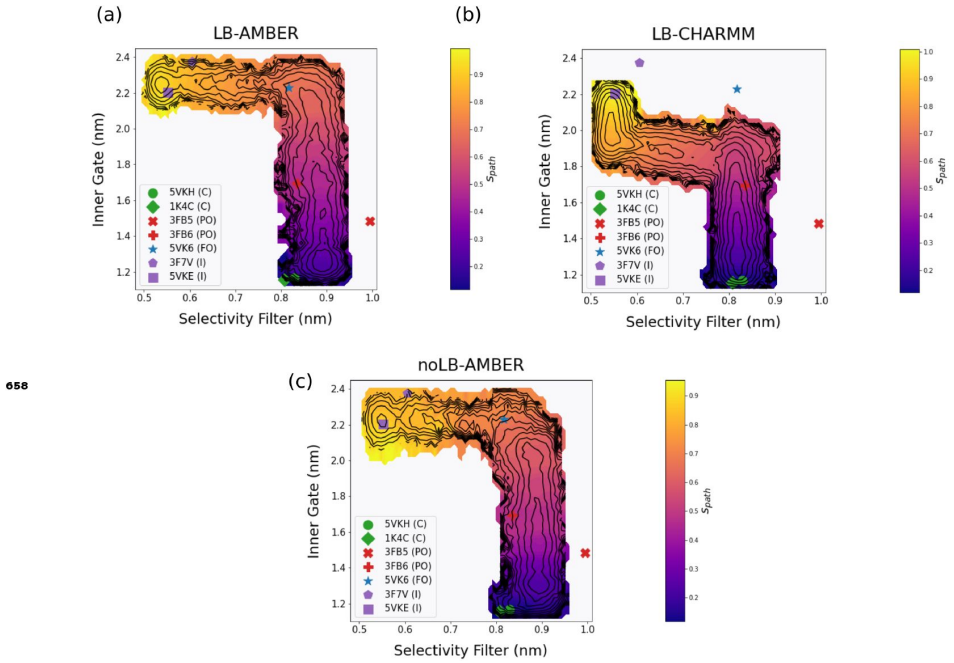

Figure 2—figure supplement 3.

The weighted average value of s_{path} projected 2D-free energy surface projected on the IG and SF. The systems represented are (a) LB-AMBER, (b) LB-CHARMM and (c) noLB-AMBER.

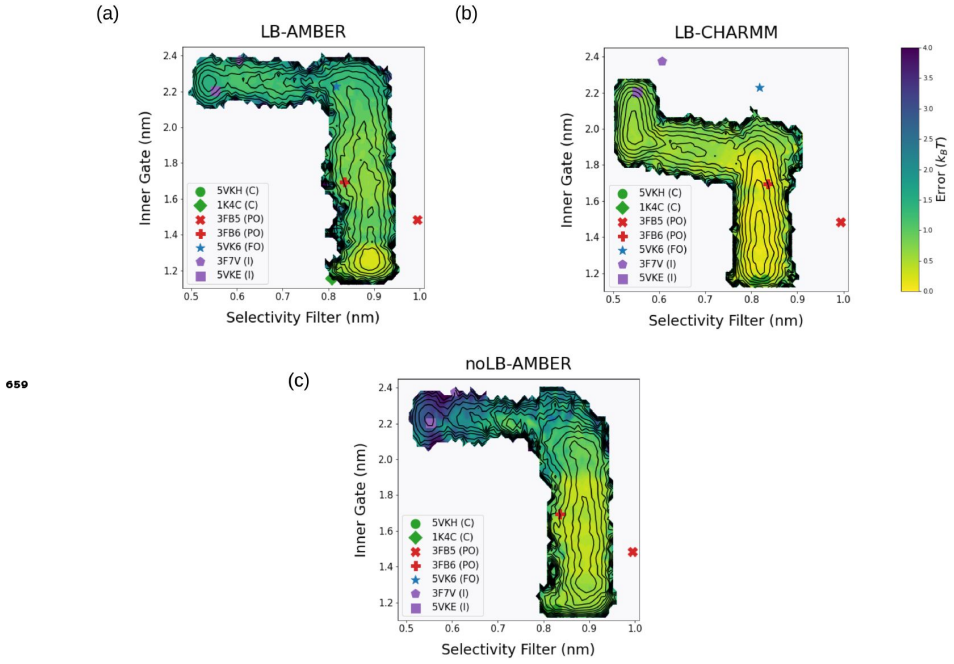

Figure 2—figure supplement 4.

Estimation of the uncertaintly associated with the 2D-free energy surface projected on the IG and SF (see Methods). The systems represented are (a) LB-AMBER, (b) LB-CHARMM and (c) noLB-AMBER.

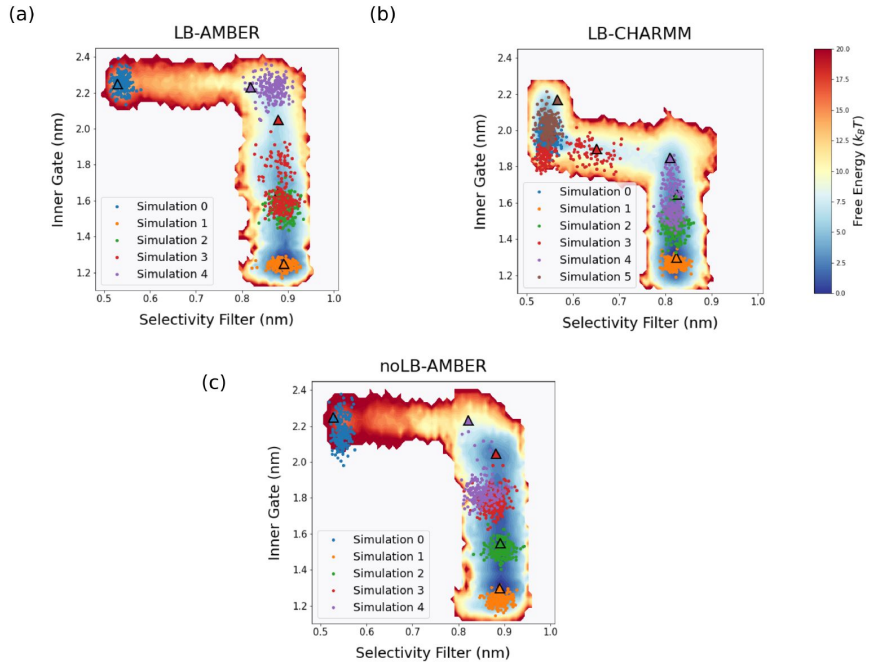

Figure 2—figure supplement 5.

IG and SF projections of 200 ns MD trajectories started from representatives of different states of the inactivation cycle onto corresponding free energy surface. The starting structure is represented as a triangle. The systems represented are (a) LB-AMBER, (b) LB-CHARMM and (c) noLB-AMBER.

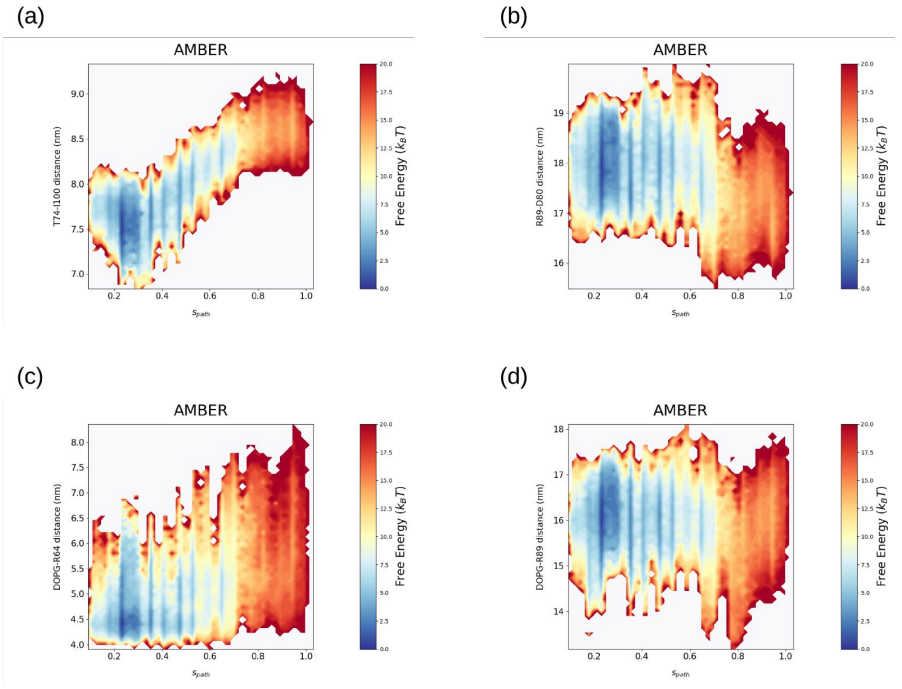

Figure 3—figure supplement 1.

Reweighted free energy surfaces calculated from the string method with swarms of trajectories of the AMBER with lipids bound system. 2D free energy surfaces projected on the path cv (s_{path}) and an additional CV of interest. These CVs of interest are: (a) T74 CA - I100 CA distance and (b) R89 CZ - D80 CG distance (c) Copurifying DOPG P - R64 CZ distance (d) Copurifying DOPG P - R89 CZ distance.

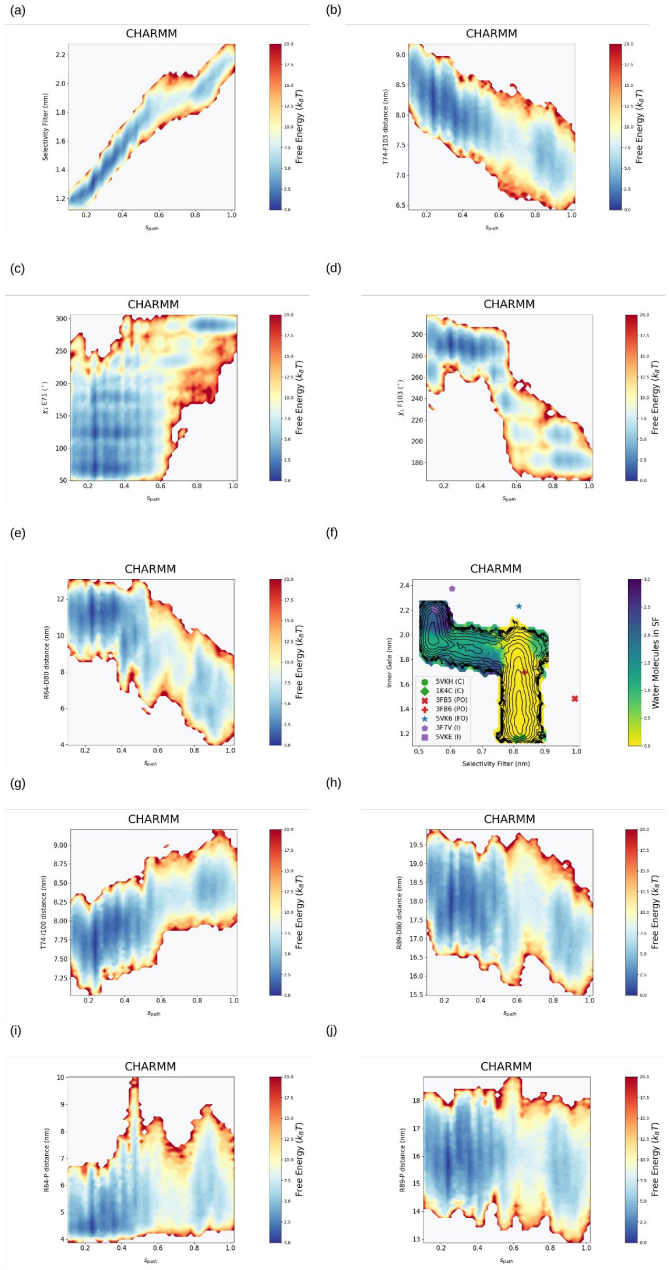

662

Figure 3—figure supplement 2.

Reweighted free energy surfaces calculated from the string method with swarms of trajectories of the CHARMM with lipids bound system. 2D free energy surfaces projected on the path cv (s_{path}) and an additional CV of interest. These CVs of interest are: (a) Inner gate distance, (b) T74 CA - F103 CA distance, (c) E71 χ_1 Janin angle, (d) F103 χ_1 Janin angle, (e) R64 CZ - D80 CG distance, (g) T74 CA - I100 CA distance and (h) R89 CZ - D80 CG distance. (f) Projected weighted average number of water molecules inside the selectivity filter (sites S1-S4) on the free energy surface of the CHARMM lipid bound system (i) Copurifying DOPG P - R64 CZ distance (j) Copurifying DOPG P - R89 CZ distance.

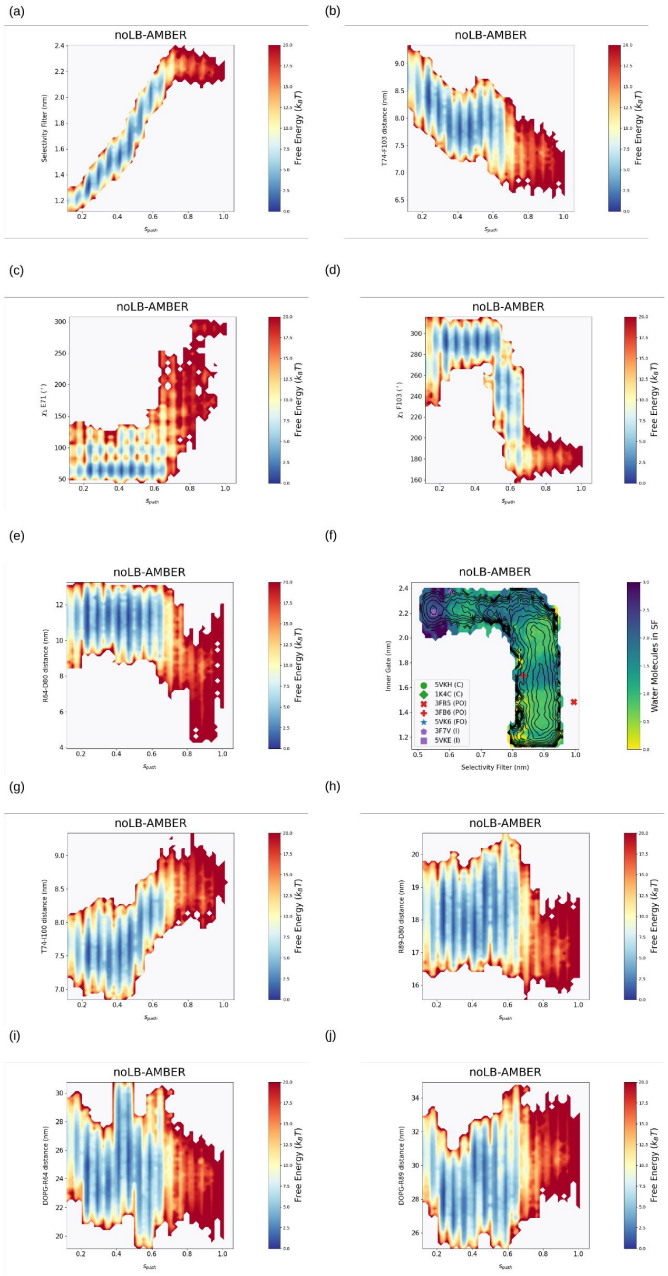

663

Figure 3—figure supplement 3.

Reweighted free energy surfaces calculated from the string method with swarms of trajectories of the AMBER without lipids bound system. 2D free energy surfaces projected on the path cv (s_{path}) and an additional CV of interest. These CVs of interest are: (a) Inner gate distance, (b) T74 CA - F103 CA distance, (c) E71 χ_1 Janin angle, (d) F103 χ_1 Janin angle, (e) R64 CZ - D80 CG distance, (g) T74 CA - I100 CA distance and (h) R89 CZ - D80 CG distance. (f) Projected weighted average number of water molecules inside the selectivity filter (sites S1-S4) on the free energy surface of the AMBER without lipid bound system (i) Copurifying DOPG P - R64 CZ distance (j) Copurifying DOPG P - R89 CZ distance.

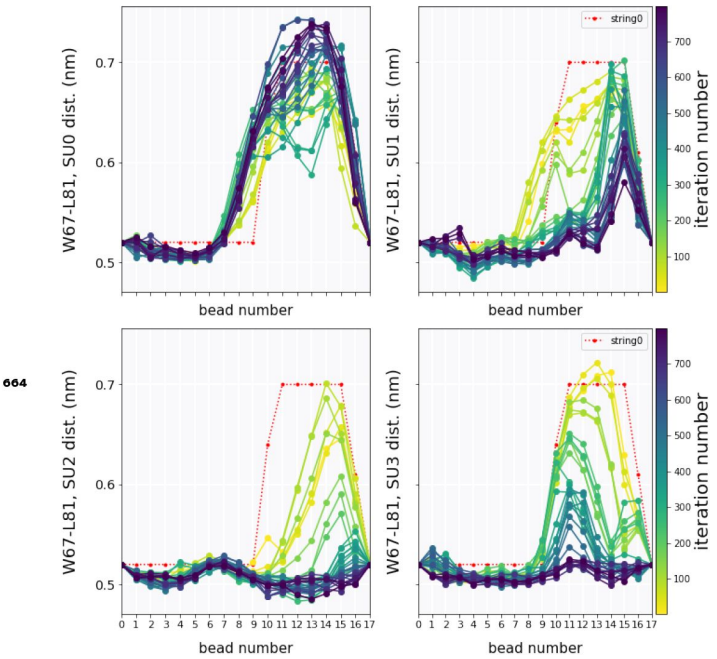

664

Figure 3—figure supplement 4.

W67-L81 distance strings as a function of the string method iteration number for the AMBER system and with each graph representing the data for a particular subunit of the tetramer.

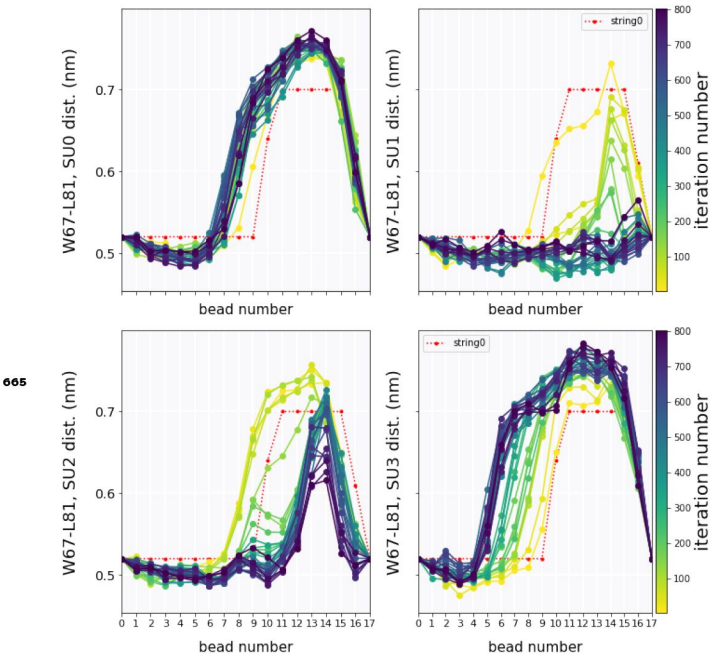

665

Figure 3—figure supplement 5.

W67-L81 distance strings as a function of the string method iteration number for the CHARMM system and with each graph representing the data for a particular subunit of the tetramer.

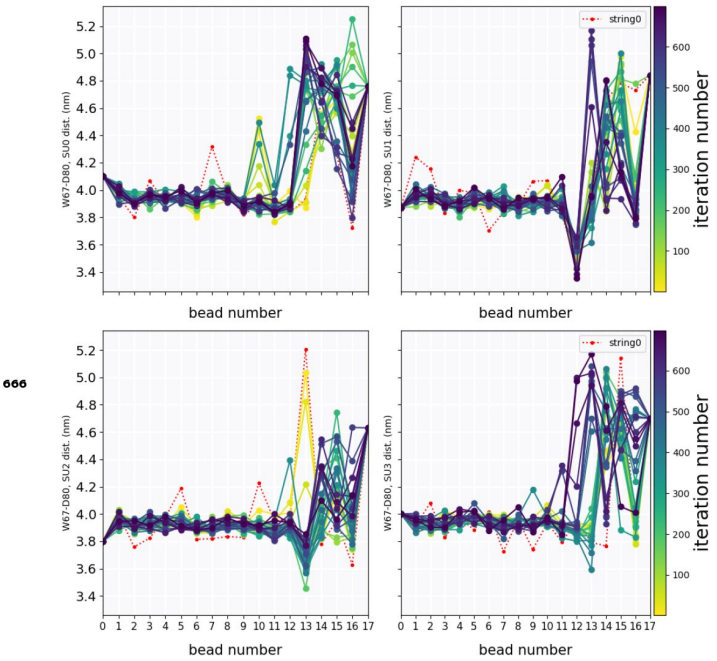

666

Figure 3—figure supplement 6.

W67-D80 distance strings as a function of the string method iteration number for the AMBER system and with each graph representing the data for a particular subunit of the tetramer.

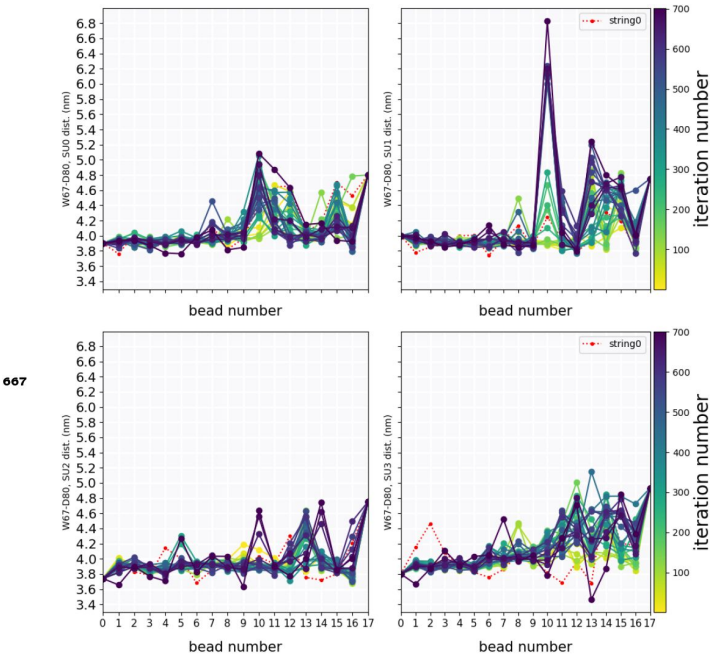

667

Figure 3—figure supplement 7.

W67-D80 distance strings as a function of the string method iteration number for the CHARMM system and with each graph representing the data for a particular subunit of the tetramer.

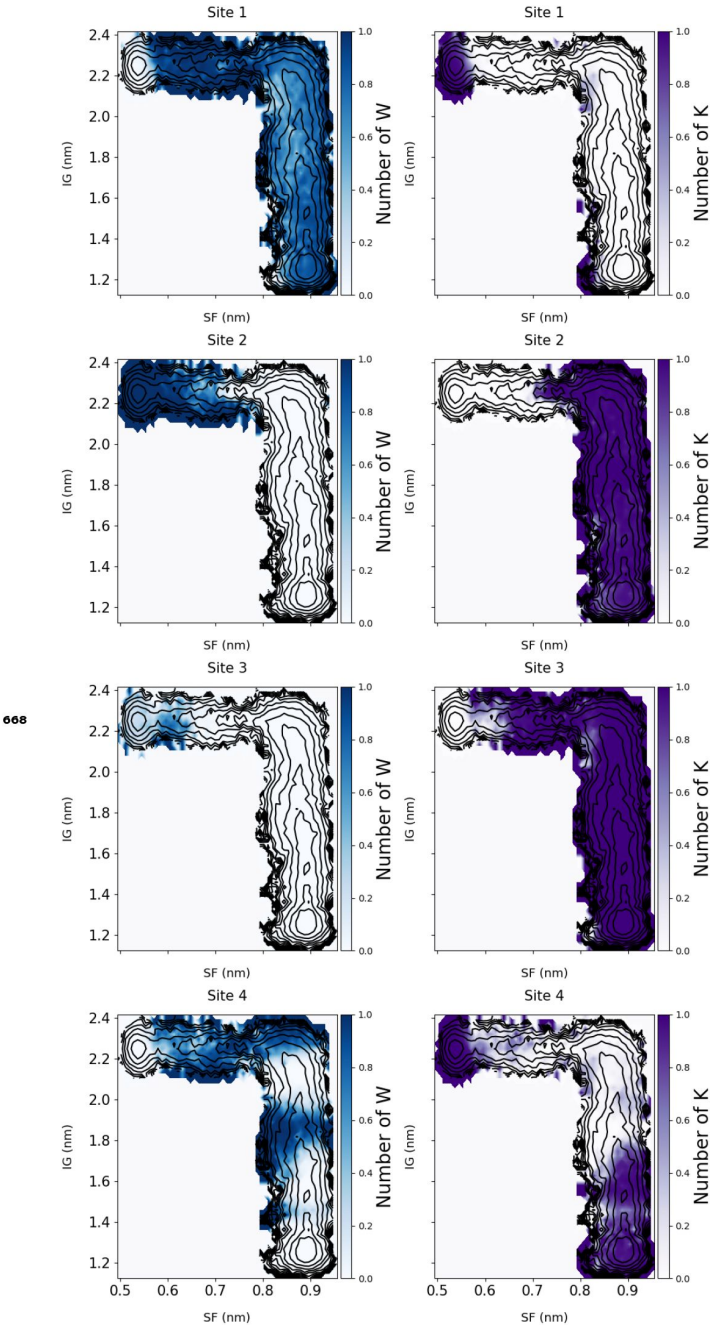

668

Figure 3—figure supplement 8.

Projected weighted average number of water molecules (blue) or potassium ions (purple) inside a particular selectivity filter sites, S1 to S4 (rows), on the IG vs SF free energy surface of the AMBER with lipid bound system.

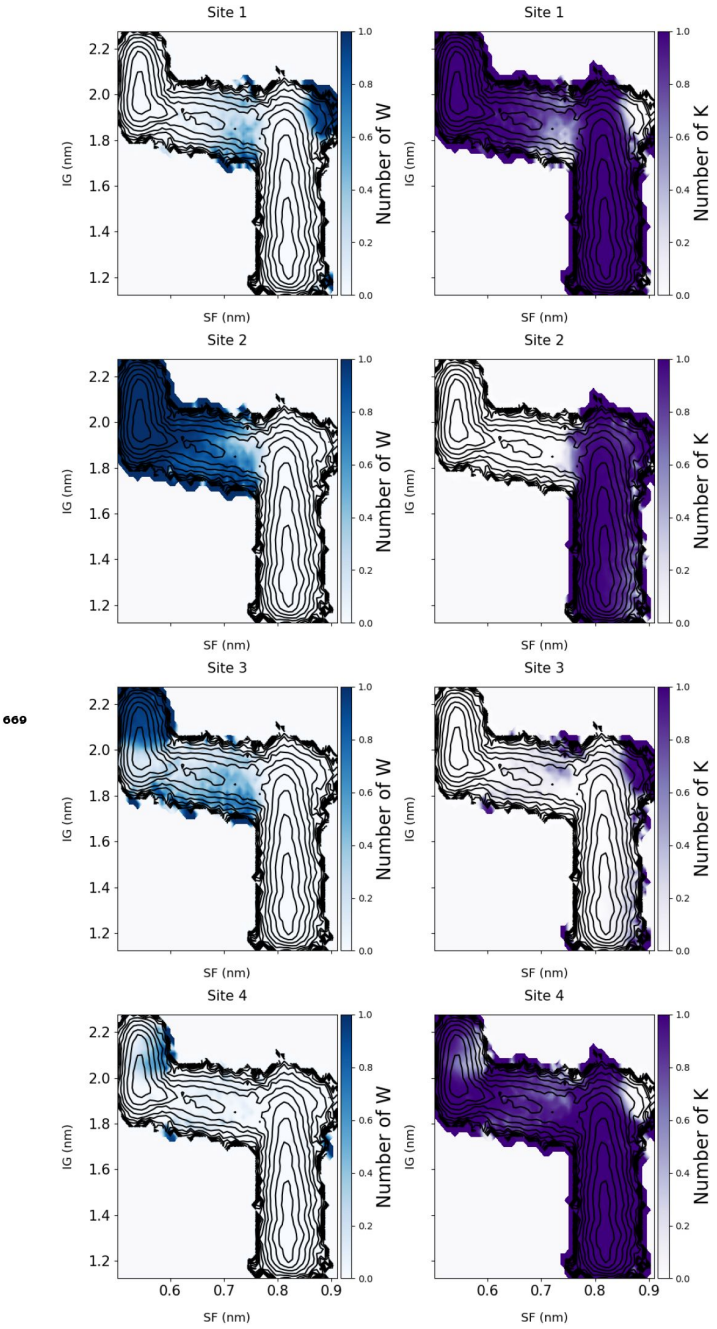

669

Figure 3—figure supplement 9.

Projected weighted average number of water molecules (blue) or potassium ions (purple) inside a particular selectivity filter sites, S1 to S4 (rows), on the IG vs SF free energy surface of the CHARMM with lipid bound system.

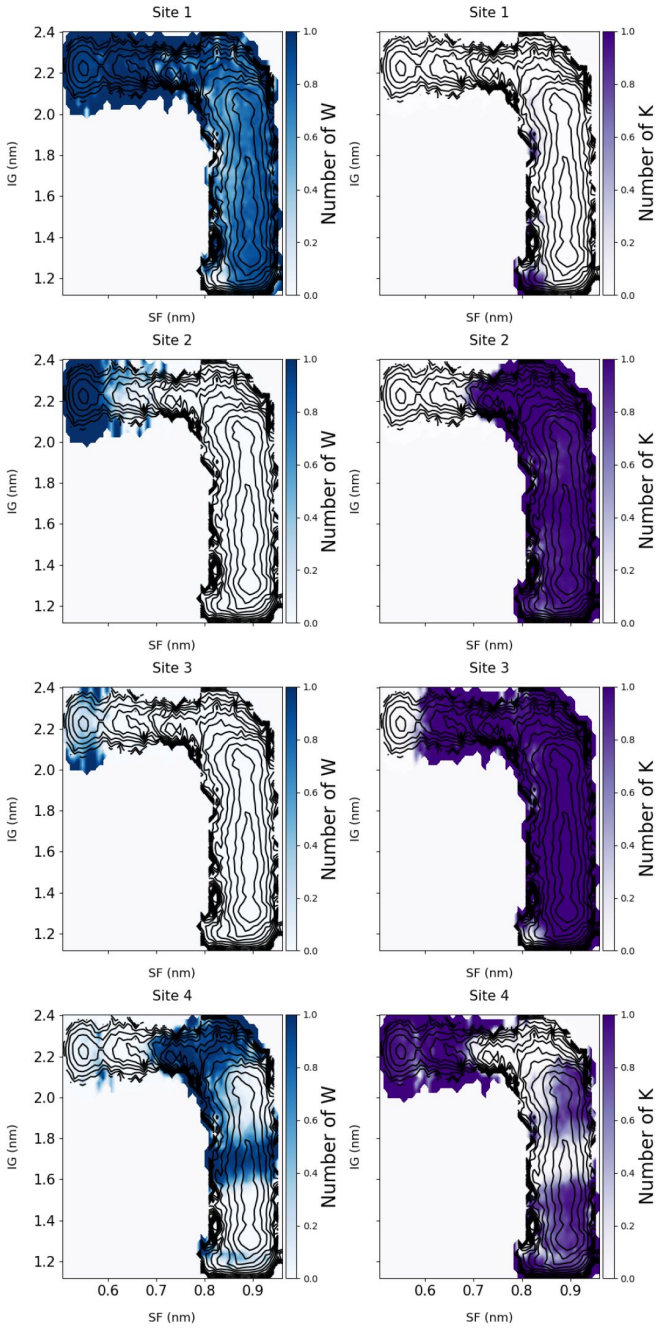

Figure 3—figure supplement 10.

Projected weighted average number of water molecules (blue) or potassium ions (purple) inside a particular selectivity filter sites, S1 to S4 (rows), on the IG vs SF free energy surface of the AMBER without lipid bound system.

References

1. Allen TW, Andersen OS, Roux B (2004) **Energetics of ion conduction through the gramicidin channel** *Proceedings of the National Academy of Sciences of the United States of America* **101**:117–122 https://doi.org/10.1073/pnas.2635314100

2. Alvis SJ, Williamson IM, East JM, Lee AG (2003) **Interactions of Anionic Phospholipids and Phosphatidylethanolamine with the Potassium Channel KcsA** *Biophysical Journal* **85**:3828–3838 https://doi.org/10.1016/S0006-3495(03)74797-3

3. Boiteux C, Posson DJ, Allen TW, Nimigean CM (2020) **Selectivity filter ion binding affinity determines inactivation in a potassium channel** *Proceedings of the National Academy of Sciences* **117**:29968–29978 https://doi.org/10.1073/pnas.2009624117

4. Branduardi D, Gervasio FL, Parrinello M (2007) **From A to B in free energy space** *Journal of Chemical Physics* **126** https://doi.org/10.1063/1.2432340

5. Bussi G, Donadio D, Parrinello M (2007) **Canonical sampling through velocity rescaling** *Journal of Chemical Physics* **126** https://doi.org/10.1063/1.2408420

6. Carnevale V, Delemotte L, Howard RJ (2021) **Molecular Dynamics Simulations of Ion Channels** *Trends in Biochemical Sciences* **46**:621–622 https://doi.org/10.1016/j.tibs.2021.04.005

7. Cordero-Morales JF, Jogini V, Chakrapani S, Perozo E (2011) **A multipoint hydrogen-bond network underlying KcsA C-type inactivation** *Biophysical journal* **100**:2387–2393

8. Cuello LG, Cortes DM, Perozo E (2017) **The gating cycle of a K+ channel at atomic resolution** *eLife* **6**:1–17 https://doi.org/10.7554/eLife.28032

9. Cuello LG, Jogini V, Cortes DM, Pan AC, Gagnon DG, Dalmas O, Cordero-Morales JF, Chakrapani S, Bt Roux, Perozo E (2010) **Structural basis for the coupling between activation and inactivation gates in K+ channels** *Nature* **466**:272–275 https://doi.org/10.1038/nature09136

10. Cuello LG, Jogini V, Cortes DM, Perozo E (2010) **Structural mechanism of C-type inactivation in K+ channels** *Nature* **466**:203–208 https://doi.org/10.1038/nature09153

11. Demmers JAA, Van Dalen A, De Kruijff B, Heck AJR, Killian JA (2003) **Interaction of the K+ channel KcsA with membrane phospholipids as studied by ESI mass spectrometry** *FEBS Letters* **541**:28–32 https://doi.org/10.1016/S0014-5793(03)00282-5

12. Doyle DA, Cabral JM, Pfuetzner RA, Kuo A, Gulbis JM, Cohen SL, Chait BT, MacKinnon R (1998) **The structure of the potassium channel: Molecular basis of K+ conduction and selectivity** *Science* **280**:69–77 https://doi.org/10.1126/science.280.5360.69

13. Fleetwood O, Carlsson J, Delemotte L (2021) **Identification of ligand-specific g-protein coupled receptor states and prediction of downstream efficacy via data-driven modeling** *eLife* **10**:1–46 https://doi.org/10.7554/eLife.60715

14. Fleetwood O, Matricon P, Carlsson J, Delemotte L (2019) **Energy landscapes reveal agonist control of GPCR activation via microswitches** *Biochemistry* :1–37 https://doi.org/10.1101/627026

15. Flood E, Boiteux C, Lev B, Vorobyov I, Allen TW (2019) **Atomistic Simulations of Membrane Ion Channel Conduction** *Gating, and Modulation. American Chemical Society* https://doi.org/10.1021/acs.chemrev.8b00630

16. Flyvbjerg H, Petersen HG (1989) **Error estimates on averages of correlated data** *The Journal of Chemical Physics* **91**:461–466 https://doi.org/10.1063/1.457480

17. Fowler PW, Abad E, Beckstein O, Sansom MSP (2013) **Energetics of multi-ion conduction pathways in potassium ion channels** *Journal of Chemical Theory and Computation* **9**:5176–5189 https://doi.org/10.1021/ct4005933

18. Furini S, Domene C (2009) **Atypical mechanism of conduction in potassium channels** *Proceedings of the National Academy of Sciences of the United States of America* **106**:16074–16077 https://doi.org/10.1073/pnas.0903226106

19. Furini S, Domene C (2020) **Critical Assessment of Common Force Fields for Molecular Dynamics Simulations of Potassium Channels** *Journal of Chemical Theory and Computation* **16**:7148–7159 https://doi.org/10.1021/acs.jctc.0c00331

20. Hille B. (2001) **Ionic channels in excitable membranes** *Current problems and biophysical approaches*

21. Hoffmann M, Scherer M, Hempel T, Mardt A, de Silva B, Husic BE, Klus S, Wu H, Kutz N, Brunton SL, Noé F (2021) **Deeptime: a Python library for machine learning dynamical models from time series data** *Machine Learning: Science and Technology* **3** https://doi.org/10.1088/2632-2153/ac3de0

22. Huang J, MacKerell ADJ (2013) **CHARMM36 all-atom additive protein force field: validation based on comparison to NMR data** *Journal of computational chemistry* **34**:2135–2145 https://doi.org/10.1002/jcc.23354

23. Huang J, Rauscher S, Nawrocki G, Ran T, Feig M, De Groot BL, Grubmüller H, MacKerell AD (2016) **CHARMM36m: An improved force field for folded and intrinsically disordered proteins** *Nature Methods* **14**:71–73 https://doi.org/10.1038/nmeth.4067

24. Hub JS, De Groot BL, Van Der Spoel D (2010) **G-whams-a free Weighted Histogram Analysis implementation including robust error and autocorrelation estimates** *Journal of Chemical Theory and Computation* **6**:3713–3720 https://doi.org/10.1021/ct100494z

25. Jämbeck JPM, Lyubartsev AP (2012) **An extension and further validation of an all-atomistic force field for biological membranes** *Journal of Chemical Theory and Computation* **8**:2938–2948 https://doi.org/10.1021/ct300342n

26. Jämbeck JPM, Lyubartsev AP (2013) **Another piece of the membrane puzzle: Extending slipids further** *Journal of Chemical Theory and Computation* **9**:774–784 https://doi.org/10.1021/ct300777p

27. Jekhmane S, Medeiros-Silva J, Li J, Kümmerer F, Müller-Hermes C, Baldus M, Roux B, Weingarth M (2019) **Shifts in the selectivity filter dynamics cause modal gating in K + channels** *Nature Communications* **10**:1–12 https://doi.org/10.1038/s41467-018-07973-6

28. Jo S, Cheng X, Lee J, Kim S, Park SJ, Patel DS, Beaven AH, Lee KI, Rui H, Park S, Lee HS, Roux B, MacKerell AD, Klauda JB, Qi Y, Im W (2017) **CHARMM-GUI 10 years for biomolecular modeling and simulation** *Journal of Computational Chemistry* **38**:1114–1124 https://doi.org/10.1002/jcc.24660

29. Kopec W, Köpfer DA, Vickery ON, Bondarenko AS, Jansen TLC, de Groot BL, Zachariae U (2018) **Direct knock-on of desolvated ions governs strict ion selectivity in K + channels** *Nature Chemistry* **10**:813–820 https://doi.org/10.1038/s41557-018-0105-9

30. Kopec W, Rothberg BS, de Groot BL (2019) **Molecular mechanism of a potassium channel gating through activation gate-selectivity filter coupling** *Nature Communications* **10**:1–15 https://doi.org/10.1038/s41467-019-13227-w

31. Kopec W, Thomson AS, de Groot BL, Rothberg BS (2022) **Driving Forces underlying Selectivity Filter Gating in the MthK Potassium Channel** *bioRxiv* https://doi.org/10.1101/2022.03.29.486236

32. Labro AJ, Marien Cortes D, Tilegenova C, Cuello LG (2018) **Inverted allosteric coupling between activation and inactivation gates in K+ channels** *Proceedings of the National Academy of Sciences of the United States of America* **115**:5426–5431 https://doi.org/10.1073/pnas.1800559115

33. Lev B, Murail S, Poitevin F, Cromer BA, Baaden M, Delarue M, Allen TW (2017) **String method solution of the gating pathways for a pentameric ligand-gated ion channel** *Proceedings of the National Academy of Sciences of the United States of America* **114**:E4158–E4167 https://doi.org/10.1073/pnas.1617567114

34. Lev B, Murail S, Poitevin F, Cromer BA, Baaden M, Delarue M, Allen TW (2017) **String method solution of the gating pathways for a pentameric ligand-gated ion channel** *Proceedings of the National Academy of Sciences of the United States of America* **114**:E4158–E4167 https://doi.org/10.1073/pnas.1617567114

35. Li J, Ostmeyer J, Cuello LG, Perozo E, Roux B (2018) **Rapid constriction of the selectivity filter underlies C-type inactivation in the KcsA potassium channel** *Journal of General Physiology* **215**:1408–1420 https://doi.org/10.1085/jgp.201812082

36. Lill MA, Danielson ML (2011) **Computer-aided drug design platform using PyMOL** *Journal of Computer-Aided Molecular Design* **25**:13–19 https://doi.org/10.1007/s10822-010-9395-8

37. Lindahl E, Sansom MSP (2008) **Membrane proteins: molecular dynamics simulations** *Current Opinion in Structural Biology* **18**:425–431 https://doi.org/10.1016/j.sbi.2008.02.003

38. Lolicato M, Natale AM, Abderemane-Ali F, Crottès D, Capponi S, Duman R, Wagner A, Rosenberg JM, Grabe M, Minor DL, . Science Advances. (2020) **K 2P channel C-type gating involves asymmetric selectivity filter order-disorder transitions**

39. Maier JA, Martinez C, Kasavajhala K, Wickstrom L, Hauser KE, Simmerling C (2015) **ff14SB: Improving the Accuracy of Protein Side Chain and Backbone Parameters from ff99SB** *Journal of Chemical Theory and Computation* **11**:3696–3713 https://doi.org/10.1021/acs.jctc.5b00255

40. Marius P, Zagnoni M, Sandison ME, Malcolm East J, Morgan H, Lee AG (2008) **Binding of anionic lipids to at least three nonannular sites on the potassium channel KcsA is required for channel opening** *Biophysical Journal* **94**:1689–1698 https://doi.org/10.1529/biophysj.107.117507

41. McComas SE, Mitrovic D, Alleva C, Bonaccorsi M, Drew D, Delemotte L (2022) **Determinants of sugar-induced influx in the mammalian fructose transporter GLUT5** *bioRxiv* https://doi.org/10.1101/2022.06.17.495601

42. Oakes V, Furini S, Domene C (2020) **Effect of anionic lipids on ion permeation through the KcsA K+-channel** *Biochimica et Biophysica Acta (BBA) - Biomembranes* **1862** https://doi.org/10.1016/j.bbamem.2020.183406

43. Ostmeyer J, Chakrapani S, Pan AC, Perozo E, Roux B (2013) **Recovery from slow inactivation in K+ channels is controlled by water molecules** *Nature* **501**:121–124 https://doi.org/10.1038/nature12395

44. Pan AC, Sezer D, Roux B (2008) **Finding transition pathways using the string method with swarms of trajectories** *Journal of Physical Chemistry B* **112**:3432–3440 https://doi.org/10.1021/jp0777059

45. Parrinello M, Rahman A (1981) **Polymorphic transitions in single crystals: A new molecular dynamics method** *Journal of Applied Physics* **52**:7182–7190 https://doi.org/10.1063/1.328693

46. Pérez-Conesa S, Keeler EG, Zhang D, Delemotte L, McDermott AE (2021) **Informing NMR experiments with molecular dynamics simulations to characterize the dominant activated state of the KcsA ion channel** *The Journal of Chemical Physics* **154**

47. Pless SA, Galpin JD, Niciforovic AP, Kurata HT, Ahern CA (2013) **Hydrogen bonds as molecular timers for slow inactivation in voltage-gated potassium channels** *Elife* **2**

48. Poveda JA, Giudici AM, Renart ML, Millet O, Morales A, González-Ros JM, Oakes V, Furini S, Domene C (2019) **Modulation of the potassium channel KcsA by anionic phospholipids: Role of arginines at the non-annular lipid binding sites** *Biochimica et Biophysica Acta - Biomembranes* **1861** https://doi.org/10.1016/j.bbamem.2019.183029

49. Reddi R, Matulef K, Riederer EA, Whorton MR, Valiyaveetil FI (2022) **Structural basis for C-type inactivation in a Shaker family voltage-gated K+ channel** *Science Advances* **8** https://doi.org/10.1126/sciadv.abm8804

50. Rohaim A, Vermeulen BJA, Li J, Kü mmerer F, Napoli F, Blachowicz L, Medeiros-Silva J, Roux B, Weingarth M (2022) **A distinct mechanism of C-type inactivation in the Kv-like KcsA mutant E71V** *Nature Communications* **13**:1–14 https://doi.org/10.1038/s41467-022-28866-9

51. Selvakumar P, Fernández-Mariño AI, Khanra N, He C, Paquette AJ, Wang B, Huang R, Smider VV, Rice WJ, Swartz KJ, et al. (2022) **Structures of the T cell potassium channel Kv1. 3 with immunoglobulin modulators** *Nature Communications* **13**

52. Tan XF, Bae C, Stix R, Fernández-Mariño AI, Huffer K, Chang TH, Jiang J, Faraldo-Gómez JD, Swartz KJ (2022) **Structure of the Shaker Kv channel and mechanism of slow C-type inactivation** *Science Advances* **8** https://doi.org/10.1126/sciadv.abm7814

53. Tan XF, Bae C, Stix R, Fernández-Mariño AI, Huffer K, Chang TH, Jiang J, Faraldo-Gómez JD, Swartz KJ (2022) **Structure of the Shaker Kv channel and mechanism of slow C-type inactivation** *Science Advances* **8** https://doi.org/10.1126/sciadv.abm7814

54. Weingarth M, Prokofyev A, Van Der Cruijsen EAW, Nand D, Bonvin AMJJ, Pongs O, Baldus M (2013) **Structural determinants of specific lipid binding to potassium channels** *Journal of the American Chemical Society* **135**:3983–3988 https://doi.org/10.1021/ja3119114

55. Westerlund AM, Fleetwood O, Pérez-Conesa S, Delemotte L (2020) **Network analysis reveals how lipids and other cofactors influence membrane protein allostery** *Journal of Chemical Physics* **153**

56. Westerlund A. M., Fleetwood O., Pérez-Conesa S., Delemotte L. (2020) **Network analysis reveals how lipids and other cofactors influence membrane protein allostery** *J. Chem. Phys.* **153** https://doi.org/10.1063/5.0020974

57. Zhang D, Howarth GS, Parkin LA, McDermott AE (2021) **NMR studies of lipid regulation of the K+ channel KcsA** *Biochimica et Biophysica Acta - Biomembranes* **1863** https://doi.org/10.1016/j.bbamem.2020.183491

Author information

Sergio Pérez-Conesa
Science for Life Laboratory, Department of Applied Physics, KTH Royal Institute of Technology, Stockholm
ORCID iD: 0000-0003-1951-2543

Lucie Delemotte
Science for Life Laboratory, Department of Applied Physics, KTH Royal Institute of Technology, Stockholm
For correspondence: lucie.delemotte@scilifelab.se
ORCID iD: 0000-0002-0828-3899

Editors

Reviewing Editor
Toby Allen
RMIT University, Australia

Senior Editor
Merritt Maduke
Stanford University School of Medicine, United States of America

Reviewer #1 (Public Review):

This manuscript employs a string method with swarms of trajectories to extract a free energy map of KcsA channel inactivation and its model dependence. The approach connects X-ray structures for closed, partially and fully open, and inactivated KcsA through optimisation of a string defined in a collective variable space consisting of distances involving gate size, cavity-filter and filter pinching (as defined in the proposed X-ray structure for an inactivated state). The final trajectory includes pore opening and filter collapse with water penetration behind

the filter, via different intermediates depending on the force field. The authors propose a role for residue L81 in controlling water entry in the final stage of this process. The results suggest that KcsA more easily inactivates with the Charmm force field, with lower barrier and direct passage from a partially open state, whereas the pathway for Amber involves transition first to a fully open state with higher barrier, despite not being the dominant open state seen experimentally under activating conditions. The results also suggest that PG lipids help activate the channel within the Amber force field, consistent with experimental evidence. The work represents large-scale advanced MD simulation. Some questions remain, however, such as if the CV space chosen is sufficient to capture all possible slow coordinates in the inactivation process, and how the resultant free energy surfaces may potentially depend on the end structures and initial pulling procedure.

Collective variable choice:

The explanation for the choice of CVs on page 5 is not sufficient to understand the process and its likely success. How were the most important and unimportant CVs identified exactly? Table 2 on page 19 shows only gate distances, cavity-filter distances and a single variable related to filter structure itself (77 CA - 77 CA) representing a pinch. Is that pinching really the only slow variable associated with inactivation changes in the filter? Why are there no variables, say for carbonyl flipping, E71 or D80 movements or even for ion and water occupancy (although water may be sampled with control of other interactions, such as involving L81)? I understand that the X-ray structure is the one source of information used to define an inactivated structure and is one with just a pinch and no complete carbonyl flipping away from the pore, as has been identified in past studies and discussed as being involved by the authors on page 14. Key changes like carbonyl flipping surely are part of the story and may be slow variables. At the very least, if not part of the CV space, could be analysed.

On page 10 the authors discuss possible differences in Amber and Charmm involving the extent to which the 4 subunits change in respect to the L81-W67 water pathway and W67-D80 hydrogen bond, arguing the different results for force field could be to do with different numbers of subunits doing different things. If I understand, the chosen CVs are all tetramer-based distances (including across subunits) and not subunit-based CVs, so that random and incomplete changes may occur to subunits for a given point in CV space. There is thus potential for the string to converge on a local minimum pathway with partial changes to its interactions within and between subunits, and may not be a unique global solution. Can the authors please explain whether or not this is possible and what analysis has been done to check it?

X-ray endpoints and initial pathway:

The string was created from a pulling/steered MD between existing X-ray structures for the closed (5VKH), partially open (3FB5), fully open (5VK6) and finally inactivated (5VKE) states. The authors write on page 12 that "The block of conduction during inactivation appears to result from pinching at the selectivity filter...", but given the end point was forced to be the X-ray structure with pinching, wasn't this outcome predetermined? This raises a significant point of how much has choice of endpoints predetermined the final states of the string? i.e. How much is an end state actually allowed to draft away from the initial Xray structure. Was a bead placed at the very endpoint and allowed to update via swarms, or was it fixed and all beads just interpolate between those fixed end states? The reason this is important is that it is plausible the inactivated crystal structure with pinching but not other changes (such as complete V76 carbonyl flipping or outer filter splaying), may not be the actual free energy minimum structure for that state and that force field.

Another obvious concern is the possible reliance on the initial pulling procedure used before string optimisation began. Fig.2 Supp 1 shows generally that the Amber path stayed pretty

close to the initial steered MD path, whereas Charmm drifted downward away from that path. One could justifiably ask, if a very different initial path was chosen, might different local minimum pathways result, including Amber sampling a path like Charmm? How does one test whether or not the final path has not been trapped in some local trough of free energy? e.g. Imagine starting the Amber string using an initial path like the more diagonal Charmm-like path, or even a more extreme unphysiological one, such as a steered trajectory that initially inactivates before opening the gate. Would the final results be the same? I appreciate the simulations are very expensive and such trials may not be possible, but what evidence is there that the final path has not been trapped away from the global minimum?

One test offered by the authors is a set of unbiased MD simulations launched from points on the string. The authors ran 200ns simulations and write on page 5 that "These simulations have the expected stability based on their starting values. This is a good quality test to check the correct estimation of the general features of the free energy surface". While this sounds reasonable, 200ns MD may only be sufficient to begin to explore locally within the solved free energy trough, much like the swarms in the iterations were able to do. My own examination of Fig2 Supp 5 is that some of these simulations linger around the expected states and some drift away within the general trough of sampling, which is a good sign. What those 200ns simulations may not be able to do is escape that trough and see evidence of other possible solutions, beyond what was sampled with the string that was tied to Xray endpoints and trapped in the solution pathway that was already formed after 100-300 iterations. Overall, the string involved 800 iterations of 10ps swarms (80ns around each bead; albeit 32 trajectories in parallel), allowing good local sampling around the beads in the free energy trough, but in terms of ability to diffuse away from that point, only being comparable in contiguous trajectory time to the unbiased MD tests. It therefore would have been interesting to see if longer simulations remain in this trough; though I understand the challenges in running so much MD. Such simulations may, however, lead to exploration beyond what was seen in the string solutions.

Force field effects and origin:

Regarding the effect of the chosen force field, the authors state that "Given that our simulations were conducted under activating conditions, we had expected the open states to be more populated than the closed ones. Simulations carried out at higher pH may be able to resolve this inconsistency". Also running at high pH would be a nice thing to do to prove the method is in fact sensitive to conditions to see a shift in the distribution of states. But the question is why were open states not more occupied under low pH and 50mM K+? From my analysis of the figures, the results show that the Charmm force field tends to allow for opening of the channel somewhat (at least with similar free energy for partially and fully open to closed) whereas Amber tends to close the channel more (with more uphill energy as the channel opens than Charmm; Fig 2). i.e. at low pH and 50 K+, isn't the Amber model incorrectly reporting fairly strong bias against opening? Moreover, regarding the free energy of the inactivated state itself, why should we not expect equilibrated channels under activating conditions to eventually fall into an inactivated state, in which case we should expect low free energy of that state (as found with Charmm and not Amber in Fig2), but with a slow rate. While much discussion in the manuscript appears to discuss limitations in Charmm (although on page 12 discussion leans either way), these factors may seem to favour Charmm over Amber.

On page 12 the authors explain the possible causes for force field dependence, although this seems limited to ion interactions, glutamate charges and dihedrals. But it would be nice to get a bit more insight into what terms may have influenced the pathway, in particular involving interactions between TM2 and the base of the selectivity filter and hydration behind the filter. Regarding ion interactions, is there a good reason to believe ions are key to the difference seen? i.e. How were ions involved differently in the state transitions involving

Amber and Charmm? The authors have noted a role for ion-carbonyl interactions. It is important that the authors explain which is the two competing models has been used and why. i.e. Off-the-shelf Charmm36 force field includes strong K+-backbone carbonyl interaction, previously seen to promote high ion occupancy, similar to Amber, whereas Lennard-Jones parameters modified to match N-methyl-acetamide and water partitioning (such as early Berneche, Noskov and Roux work) reduce ion occupancy and increase water content inside the filter.

Reviewer #2 (Public Review):

The authors describe a computational study into the energetics of KcsA inactivation. Using enhanced sampling, a converged free energy landscape of the inactivation process is achieved in two modern molecular mechanics force fields. The obtained profiles confirm the literature finding of too rapid inactivation, in particular in simulations using the CHARMM force field. Interestingly, it is found that selectivity filter collapse does not gradually follow opening of the inner gate, but proceeds rather switch-like. A key role for residue L81 is proposed as opening gateway in this process.

The study is impressive and interesting. However, I have a number of concerns that the authors may wish to address in a revised version of the manuscript.

First, concerning a set of unbiased simulations spawned at different regions of the investigated free energy landscapes, the authors write: "These simulations have the expected stability based on their starting values".
Fig 2.c shows a rather smooth downhill slope in the free energy curve towards the closed state for AMBER , so wouldn't the expected behavior in that case be that all unbiased trajectories end up in the closed state, or at least travel a substantial amount in that direction? However, that is not observed. This should be further investigated.

Second, "This suggests that stabilization of the partially open state by the removal of bound lipids can explain the increase in open probability" is an odd statement, as "stabilization of the partially open state" means almost the same as "increase in open probability".

The statement "both force fields yield inactivation barriers that are orders of magnitude lower than what is expected from electrophysiology experiments" seems inaccurate. Perhaps the authors mean "inactivation rates that are orders of magnitude lower" rather than barriers?

In addition, the assertion "The CHARMM force field, on the other hand, results in landscapes in agreement with the fact that one of the dominant states in activating conditions is the partially open state, as revealed by a combination of ssNMR+MD." seems to hold for the AMBER force field without PG lipids rather than for CHARMM?

Together with the higher barrier towards the inactivated state as well as covering most known x-ray structures along the inactivation pathway, this would seem to point all in the direction that the studied AMBER force field provides a more faithful picture of the inactivation pathway than CHARMM. I, therefore, find the somewhat inconclusive summary as presented in Fig. 5 a bit uninformative, as it suggests that both mechanisms might be equally likely.

Overall, the study would benefit from a follow-up step to become more conclusive. This could be either in the form of the suggested L81 mutation or changing the simulation conditions to inactivating conditions such as low salt, in which case the inactivated state would be expected to become a minimum, which would provide an additional reference point for validation. Either of these would narrow down the spectrum of possible mechanisms.

Reviewer #3 (Public Review):

The computational study reported in the manuscript "Free energy landscapes of KcsA inactivation" by Pérez-Conesa and Delemotte is quite interesting and insightful.

The computations provide the first complete analysis of how the opening of the activation gate and the constriction of the selectivity filter are coupled in the KcsA channel.

The analysis is careful and is state-of-the-art. The results reveal remarkable differences between the CHARMM and AMBER force fields.

Unfortunately, the "elephant in the room" with regards to K+ channel inactivation is the significance of the dilated structures more recently obtained by Xray and EM. While it is worthwhile doing our best to really understand the constriction mechanism of KcsA, and the present manuscript does an excellent job at that, the ground has shifted and understanding finer points about KcsA constriction has become, unfortunately, not the most prominent issue in the field at the present time.

Let's discuss the current situation about the inactivation of K+ channels. The situation is fairly unsettled. The KcsA channel was the first for which some atomic structure and mechanism, centered on a constriction of the selectivity filter, were proposed. The constricted conformation really does not conduct because the filter is too narrow. More recently a few structures (Xray and EM) for channel mutants known to have more propensity to inactivate have revealed a different conformation of the filter which appears to be dilated toward the extracellular side. This is a conformation that had never been seen previously. Different "camps" co-exist in the K+ channel community about inactivation. Those who were very skeptical about the constricted conformation claim that the new dilated structures is the final truth. While the dilated structures are certainly part of the body of information that we have now, but their significance remains somewhat unclear if anything because of the fact that they are not perfectly occluded and they allow ion conduction! While it is worthwhile doing our best to really understand the constriction mechanism of KcsA, and the present manuscript does an excellent job at that, the ground has shifted and understanding finer points about KcsA constriction has become, unfortunately, not the most prominent issue in the field at the present time.

Author Response:

> ### *Reviewer #1 (Public Review):*
>
> *[...] Collective variable choice:*
>
> *The explanation for the choice of CVs on page 5 is not sufficient to understand the process and its likely success. How were the most important and unimportant CVs identified exactly? Table 2 on page 19 shows only gate distances, cavity-filter distances and a single variable related to filter structure itself (77 CA - 77 CA) representing a pinch. Is that pinching really the only slow variable associated with inactivation changes in the filter? Why are there no variables, say for carbonyl flipping, E71 or D80 movements or even for ion and water occupancy (although water may be sampled with control of other interactions, such as involving L81)?*

CVs for steering simulations were selected based on structural comparisons between the X-ray structures as well as the information about the inactivation available in the literature. These steering CVs were later used as CVs for the string method with the exception of those

found to be irrelevant in preliminary string simulations (see methods for details). For example we discarded CVs that would just oscillate freely and thus represent fast equilibrating CVs. We will add additional explanations to the methods section of the manuscript in revisions.

Carbonyl flipping, E71 and D80 movement and SF occupancy were observed in the initial steering simulation to correlate with the 77 CA - 77 CA opening and the opening of the L81-W67 contact. They were not biased but followed the expected path as a consequence of the motion of the imposed selectivity filter constriction. Therefore, they did need not be explicitly biased. The same can be said with respect to water occupancy behind the selectivity filter, which correlates with the opening of the L81-W67 contact.

> *I understand that the X-ray structure is the one source of information used to define an inactivated structure and is one with just a pinch and no complete carbonyl flipping away from the pore, as has been identified in past studies and discussed as being involved by the authors on page 14. Key changes like carbonyl flipping surely are part of the story and may be slow variables. At the very least, if not part of the CV space, could be analysed.*

Indeed, the reviewer is correct in stating that there are molecular motions of interest aside from the ones included in the CV space. Figure 3 and associated supplementary figures indeed extensively investigate the probability distributions of many of those as the system progresses along the inactivation pathway. These results are presented in the section titled “Free energy landscapes offer insights into atomistic-resolution mechanistic details”. Carbonyl flipping seemed to be highly correlated with the 77CA- 77CA distance and this analysis was therefore not presented.

> *On page 10 the authors discuss possible differences in Amber and Charmm involving the extent to which the 4 subunits change in respect to the L81-W67 water pathway and W67-D80 hydrogen bond, arguing the different results for force field could be to do with different numbers of subunits doing different things. If I understand, the chosen CVs are all tetramer-based distances (including across subunits) and not subunit-based CVs, so that random and incomplete changes may occur to subunits for a given point in CV space.*

In fact, some of the CVs represent intrasubunit distances, for example L81-W67 while others represent distance across subunits. This distinction never represented a criterion to select CVs.

> *There is thus potential for the string to converge on a local minimum pathway with partial changes to its interactions within and between subunits, and may not be a unique global solution. Can the authors please explain whether or not this is possible and what analysis has been done to check it?*

This indeed represent a well-recognized shortcoming of all string-based enhanced sampling methods. The string-of-swarms method used herein indeed assumes that there is a dominant minimum free energy path and requires a reasonable starting path. One major advantage of this methodological choice, however, is that the path can be described in high dimension, thus avoiding stark dimensionality reduction as is the case in many collective-variable based methods such as metadynamics.

We do note that though the initial path was the same for the two force fields, the final pathway is different, which tends to indicate that the results do not only depend on the initial path but also on the force field guiding the dynamics of the process.

X-ray endpoints and initial pathway:

The string was created from a pulling/steered MD between existing X-ray structures for the closed (5VKH), partially open (3FB5), fully open (5VK6) and finally inactivated (5VKE) states. The authors write on page 12 that "The block of conduction during inactivation appears to result from pinching at the selectivity filter…", but given the end point was forced to be the X-ray structure with pinching, wasn't this outcome predetermined? This raises a significant point of how much has choice of endpoints predetermined the final states of the string? i.e. How much is an end state actually allowed to draft away from the initial Xray structure. Was a bead placed at the very endpoint and allowed to update via swarms, or was it fixed and all beads just interpolate between those fixed end states? The reason this is important is that it is plausible the inactivated crystal structure with pinching but not other changes (such as complete V76 carbonyl flipping or outer filter splaying), may not be the actual free energy minimum structure for that state and that force field.

The reviewer is right to point out that this observation is most likely a consequence of the choice of the end points of the initial string. The string method assumes that the end points of the string are fairly representative of the initial and final states of the processed studied. In this case, for ease of use, the endpoints of the simulation were fixed. When endpoints are left free to relax, they drift towards the closest minima and make comparisons between force fields, between simulation conditions, etc more difficult.

We do agree that the selection of initial and final states as well as the starting string are important modeling choices. For this reason, we were very mindful and made these choices based on the existing published evidence (available at the time).

We will make these details explicit in a revised version of the manuscript.

Another obvious concern is the possible reliance on the initial pulling procedure used before string optimisation began. Fig.2 Supp 1 shows generally that the Amber path stayed pretty close to the initial steered MD path, whereas Charmm drifted downward away from that path. One could justifiably ask, if a very different initial path was chosen, might different local minimum pathways result, including Amber sampling a path like Charmm? How does one test whether or not the final path has not been trapped in some local trough of free energy? e.g. Imagine starting the Amber string using an initial path like the more diagonal Charmm-like path, or even a more extreme unphysiological one, such as a steered trajectory that initially inactivates before opening the gate. Would the final results be the same? I appreciate the simulations are very expensive and such trials may not be possible, but what evidence is there that the final path has not been trapped away from the global minimum?

As stated above, the reviewer is right to point out the weakness of the method of converging to the closest local minimum free energy path. It is unfortunately computationally infeasible to test many possible paths. For this reason, we chose to initiate our calculations with a pathways based on experimental data; in this case based on available X-ray structures. In addition, it is necessary to contrast the results of the simulation with available experimental evidence: the string method with swarms of trajectories, when aptly used, has a history of bringing useful insights to several biological systems (Lev et al. 2017b; Suh et al. 2019, Fleetwood et al 2021, 2019; McComas et al. 2022).

As already noted, the fact that the two force field yield very different energy landscapes is evident since they would otherwise converge to the same final pathway given the same initial pathway guess.

> *One test offered by the authors is a set of unbiased MD simulations launched from points on the string. The authors ran 200ns simulations and write on page 5 that "These simulations have the expected stability based on their starting values. This is a good quality test to check the correct estimation of the general features of the free energy surface". While this sounds reasonable, 200ns MD may only be sufficient to begin to explore locally within the solved free energy trough, much like the swarms in the iterations were able to do. My own examination of Fig2 Supp 5 is that some of these simulations linger around the expected states and some drift away within the general trough of sampling, which is a good sign. What those 200ns simulations may not be able to do is escape that trough and see evidence of other possible solutions, beyond what was sampled with the string that was tied to Xray endpoints and trapped in the solution pathway that was already formed after 100-300 iterations. Overall, the string involved 800 iterations of 10ps swarms (80ns around each bead; albeit 32 trajectories in parallel), allowing good local sampling around the beads in the free energy trough, but in terms of ability to diffuse away from that point, only being comparable in contiguous trajectory time to the unbiased MD tests. It therefore would have been interesting to see if longer simulations remain in this trough; though I understand the challenges in running so much MD. Such simulations may, however, lead to exploration beyond what was seen in the string solutions.*

We agree with the authors that longer simulations would be very interesting to understand the behavior of the string-of-swarms method and how it behaves for this intricate FES. Note however, that 80 ns divided over 32 trajectories yields an overall trajectory length that is ~two orders of magnitude below a single 200 ns-long simulation. We thus still stand by our statement that the fact that these simulations behave as expected from the free energy landscapes is a good quality check of the CVs and of the resulting free energy landscapes.

> *Force field effects and origin:*
>
> *Regarding the effect of the chosen force field, the authors state that "Given that our simulations were conducted under activating conditions, we had expected the open states to be more populated than the closed ones. Simulations carried out at higher pH may be able to resolve this inconsistency". Also running at high pH would be a nice thing to do to prove the method is in fact sensitive to conditions to see a shift in the distribution of states.*

Indeed this is the logical next step for future work.

> *But the question is why were open states not more occupied under low pH and 50mM K+? From my analysis of the figures, the results show that the Charmm force field tends to allow for opening of the channel somewhat (at least with similar free energy for partially and fully open to closed) whereas Amber tends to close the channel more (with more uphill energy as the channel opens than Charmm; Fig 2). i.e. at low pH and 50 K+, isn't the Amber model incorrectly reporting fairly strong bias against opening? Moreover, regarding the free energy of the inactivated state itself, why should we not expect equilibrated channels under activating conditions to eventually fall into an inactivated state, in which case we should expect low free energy of that state (as found with Charmm and not Amber in Fig2), but with a slow rate. While much discussion in the manuscript appears to discuss limitations in Charmm (although on page 12 discussion leans either way), these factors may seem to favour Charmm over Amber.*

We would like to thank the reviewer for raising these points. We can only speculate about what might be the reasons for these discrepancies, and we have tried to be as honest as

possible in our manuscript and avoid overinterpretation of our results. It is interesting that Reviewer 2 gathered from our data that the AMBER results were more consistent with expectations while this reviewer thought the opposite. This does reinforce our decision to avoid taking sides and present both options. Our personal opinion is currently that both force fields are imperfect at describing all the aspects of the activation-inactivation gates coupling. We will include more discussion in the revisions of the manuscript.

> *On page 12 the authors explain the possible causes for force field dependence, although this seems limited to ion interactions, glutamate charges and dihedrals. But it would be nice to get a bit more insight into what terms may have influenced the pathway, in particular involving interactions between TM2 and the base of the selectivity filter and hydration behind the filter. Regarding ion interactions, is there a good reason to believe ions are key to the difference seen? i.e. How were ions involved differently in the state transitions involving Amber and Charmm? The authors have noted a role for ion-carbonyl interactions.*

We agree that this would be interesting, but judged that this would be better done in a separate study. We do note that the K-carbonyl interactions have been reported as candidates for these discrepancies, as mentioned and cited in the manuscript. Very recent simulations using ab initio MD support that the overstimation of the K-carbonyl interaction is the reason for the low conductance of potassium channels in classical MD, refer to Hui et al. Biophysical Journal, vol. 122, issue 3, p. 520a. We will add this reference in revisions.

> *It is important that the authors explain which is the two competing models has been used and why. i.e. Off-the-shelf Charmm36 force field includes strong K+-backbone carbonyl interaction, previously seen to promote high ion occupancy, similar to Amber, whereas Lennard-Jones parameters modified to match N-methyl-acetamide and water partitioning (such as early Berneche, Noskov and Roux work) reduce ion occupancy and increase water content inside the filter.*

We have used “off-the-shelf” or conventional CHARMM36 as described in the literature cited.

> ### *Reviewer #2 (Public Review):*
>
> *[...] The study is impressive and interesting. However, I have a number of concerns that the authors may wish to address in a revised version of the manuscript.*
>
> *First, concerning a set of unbiased simulations spawned at different regions of the investigated free energy landscapes, the authors write: "These simulations have the expected stability based on their starting values".*
>
> *Fig 2.c shows a rather smooth downhill slope in the free energy curve towards the closed state for AMBER , so wouldn't the expected behavior in that case be that all unbiased trajectories end up in the closed state, or at least travel a substantial amount in that direction? However, that is not observed. This should be further investigated.*

It is true that this would be the effect we should observe after a significant simulation time. Resorting to 200ns-long simulations, our goal was to test whether the local free energy basins identified by the string-of-swarms method were indeed metastable. If that were the case, we would expect the trajectories to remain within the basins on medium timescales due to the kinetic barriers that would need to be overcome to transfer to other basins. Of course, if simulations were long enough, all basins would eventually be explored by the trajectory with a probability related to the relative free energy of the basins.

> *Second, "This suggests that stabilization of the partially open state by the removal of bound lipids can explain the increase in open probability" is an odd statement, as "stabilization of the partially open state" means almost the same as "increase in open probability".*

It is true that one appears to necessarily imply the other. An increase in open probability could potentially come from two effects: a stabilization of the open state or a destabilization of the closed one. In a two-state system, the two cases are indistinguishable since only relative difference in free energies matter. However, this is a three state system, if one takes as a reference the energy of the inactivated state, there is an effective difference in the physics of the system if a stabilization of the open state or a destabilization of the closed state occurs.

> *The statement "both force fields yield inactivation barriers that are orders of magnitude lower than what is expected from electrophysiology experiments" seems inaccurate. Perhaps the authors mean "inactivation rates that are orders of magnitude lower" rather than barriers?*

Yes, this was a mistake on our part. We will amend the manuscript.

> *In addition, the assertion "The CHARMM force field, on the other hand, results in landscapes in agreement with the fact that one of the dominant states in activating conditions is the partially open state, as revealed by a combination of ssNMR+MD." seems to hold for the AMBER force field without PG lipids rather than for CHARMM?*

AMBER simulations with or without bound PG lipids have a fully open state basin within the minimum free energy path (Fig 4a, 4b) which is not the case for CHARMM (Fig 2b). In that sense, the CHRAMM force field seems to be in better agreement with the ssNMR data. The ssNMR+MD study however suggests that the PO open state basin should be the lowest in free energy. In both cases, however, the C basin is lower in free energy than the PO. We can only speculate about why that may be.

> *Together with the higher barrier towards the inactivated state as well as covering most known x-ray structures along the inactivation pathway, this would seem to point all in the direction that the studied AMBER force field provides a more faithful picture of the inactivation pathway than CHARMM. I, therefore, find the somewhat inconclusive summary as presented in Fig. 5 a bit uninformative, as it suggests that both mechanisms might be equally likely.*

Although the X-ray structures do suggest an AMBER-like path, structural information in isolation is not sufficient to fully understand a phenomenon of dynamical nature. The X-ray structures of metastable structures particularly of open states require the use of engineered mutations and other techniques to trap these states. We of course do not question that a lot of very valuable information can be derived from them, but they should be considered in the context of other computational and experimental techniques. We believe we are very explicit in the text in discussing the weakness and strengths of either possibilities. In fact, we find it interesting that Reviewer 1 gathered from our data that the CHARMM results were more consistent with expectations. This does reinforce our decision to avoid taking sides and present both options. Our personal opinion is currently that both force fields are imperfect at describing all the aspects of the activation-inactivation gates coupling.

> *Overall, the study would benefit from a follow-up step to become more conclusive. This could be either in the form of the suggested L81 mutation or changing the simulation*

conditions to inactivating conditions such as low salt, in which case the inactivated state would be expected to become a minimum, which would provide an additional reference point for validation. Either of these would narrow down the spectrum of possible mechanisms.

We absolutely agree with this reviewer. These are great suggestions for further investigations that will definitely be considered in future studies.

Reviewer #3 (Public Review):

[...] The analysis is careful and is state-of-the-art. The results reveal remarkable differences between the CHARMM and AMBER force fields.

Unfortunately, the "elephant in the room" with regards to K+ channel inactivation is the significance of the dilated structures more recently obtained by Xray and EM. While it is worthwhile doing our best to really understand the constriction mechanism of KcsA, and the present manuscript does an excellent job at that, the ground has shifted and understanding finer points about KcsA constriction has become, unfortunately, not the most prominent issue in the field at the present time.

Let's discuss the current situation about the inactivation of K+ channels. The situation is fairly unsettled. The KcsA channel was the first for which some atomic structure and mechanism, centered on a constriction of the selectivity filter, were proposed. The constricted conformation really does not conduct because the filter is too narrow. More recently a few structures (Xray and EM) for channel mutants known to have more propensity to inactivate have revealed a different conformation of the filter which appears to be dilated toward the extracellular side. This is a conformation that had never been seen previously. Different "camps" co-exist in the K+ channel community about inactivation. Those who were very skeptical about the constricted conformation claim that the new dilated structures is the final truth. While the dilated structures are certainly part of the body of information that we have now, but their significance remains somewhat unclear if anything because of the fact that they are not perfectly occluded and they allow ion conduction! While it is worthwhile doing our best to really understand the constriction mechanism of KcsA, and the present manuscript does an excellent job at that, the ground has shifted and understanding finer points about KcsA constriction has become, unfortunately, not the most prominent issue in the field at the present time.

We appreciate the reviewer's comments and we are also grateful for the contextualization of the current state of the literature with respect to KcsA inactivation.

Although we acknowledge the importance of these new findings and look forward to a lively debate in the literature regarding the importance of this alternative mechanism, this information was not available at the time when this study was started. In any case, for an initial study with a novel technology and with methodological choices such as the force field choice, studying the more established path seems still a valid choice. Of course, the techniques used to study this method can be used to study new hypotheses and contrast them with our current work. This will be an important line of work going forward. We will add further literature discussion to the manuscript and better outline how we decided on the scope of this study.